Organic & Biomolecular Chemistry

Recent synthetic methods involving carbon radicals generated by electrochemical catalysis

SCHOLARONE™
Manuscripts

Recent synthetic methods involving carbon radicals generated by electrochemical catalysis

Phuc H. Pham, [†] **Haley A. Petersen,** [†] **Jaclyn L. Katsirubas,** [†] **Oana R. Luca** [†*]

[†] *Department of Chemistry, University of Colorado Boulder and the Renewable and Sustainable*

Energy Institute, Boulder CO, 80300 USA

Phone: 1-(303) 739-6721

*E-mail: oana.luca@colorado.edu

Abstract

Driven by a resurgence of interest in electrode-driven synthetic methods, this paper covers recent activity in the field of mediated electrochemical and photoelectrochemical bond activation, inclusive of C-H, C-C, C-N, and other C–heteroatom bonds.

1. Introduction

The addition and removal of electrons through the use of change of potential or current at an electrode surface has emerged as a strategy for the development of new synthetic disconnections in organic, inorganic and organometallic synthesis.[1, 2] The use of electrical current or voltage allows for generation of highly energetic oxidizers or reductants that can in turn participate in chemical reactions. Electrochemical methods therefore avoid the use of energetic reagents that often require special safety precautions for use, handling, and disposal.

Ohm's Law. In order to understand the quantification of number of electrons and holes in the electrochemical experiment, we first need to understand some basic relationships between voltage, current and the underlying resistance. The first relationship we will look at is Ohm's law: Eq 1. The term V is the voltage (measured in Volts V, also interchangeably referred to as potential), which is directly proportional to a term I which is the current (units in Amperes A or Coulombs C per second) being passed in a chemical experiment. In Ohm's law R is the resistance of the system (measured in Ohms Ω). R is a combination of the inherent resistance of the electrochemical cell/separators/solvent and the chemical reaction itself which is, in effect, a resistance being overcome during the experiment.

$$V = I * R \qquad\qquad\qquad \text{Eq 1}$$

In an electrochemical experiment, R is almost never measured. However, its presence and importance cannot be understated. Resistance measurements are crucial in addressing experimental design issues such as resistive heating and limitations in holding experimental parameters constant throughout the experiment such as exceeding compliance of the electrochemical instrumentation.

The relationship between voltage and current can be explained through an analogy with a faucet with variable diameter. The current in coulombs per second is a measure of charge passed over a unit of time, in effect being directly analogous to the rate of flow of water out of the faucet. On the other hand, a voltage change in relationship to a current I would be analogous to changing the diameter of the faucet. A higher voltage i.e. a larger faucet diameter would allow for a higher current/flow of water to pass.

Faraday's Law. An additional useful mathematical relationship is shown in Eq 2. These equations allow us to quantify the overall charge passed Q (in units of Coulombs) as the integral of the current (in units of Coulombs/s) change over time when keeping the voltage constant. The charge passed in an experiment is related to the number of moles of electrons or holes delivered to the system through Faraday's Law (Eq 2). Q is therefore equal to the number of moles of reactant transformed multiplied by Faraday's constant 96485 C/mol and the number of total electron equivalents exchanged in a transformation.

$$Q = \int I \mathrm{d}t = \# \, of \; moles \; *nF \qquad\qquad\qquad Eq \; 2$$

Equipment and cell design. The preparative scale electrochemical synthesis is commonly called an electrolysis – simply meaning that there is a change induced in the system through the passage of electricity. Electrolysis experiments are conducted in electrochemical cells, often just simple glass vessels and vials with the use of electrodes which can be made of different types of conductive materials. The electrodes are connected to a potentiostat or a power source using wires. The power source or potentiostat in turn, may be attached to a computer, but that is not necessary especially in the case of a controlled current electrolysis, in which there is no requirement to use a reference electrode (Figure 1a). Several designs for electrochemical cells are known and many of them are available commercially. Electrochemical synthesis can be conducted by holding either the current or voltage fixed. An electrolysis conducted while holding the voltage constant is a controlled potential electrolysis (CPE) (Figure 1b), while an electrolysis at constant current is commonly abbreviated CCE (Figure 1a). CPE is executed with the use of a computer-connected potentiostat and requires the use of a reference electrode. The reference electrode is used as a static potential comparison in this experiment, and it is imperative that the reference not change during the experiment.
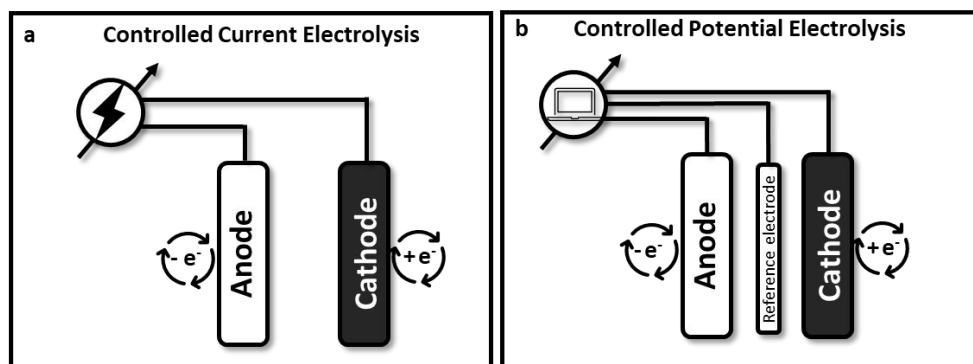
Figure 1. a. Schematic of a controlled current electrolysis setup shown as undivided. b. Schematic of a controlled potential electrolysis.

Diagnostics and analogy with chemical redox reactions. A useful diagnostic technique in electrochemical measurements is cyclic voltammetry, also known as CV. Several resources are available to introduce the reader to the technique.[3, 4] Cyclic voltammetry may be used to determine either reduction or oxidation potentials for various different types of chemical compounds, as long as they are freely diffusing in solution. These potentials are useful in comparing the relative oxidizing or reducing strength of chemical species through the mapping of redox potentials.

A ranking of formal redox potentials for various redox reagents has been previously reported.[1] Additionally, CVs may be used as a useful tool to screen for catalytic activity. A multi-fold increase in current responses at otherwise "duck-shaped" reversible waves is a quick diagnostic for catalytic response. When observed, the screening experiment is followed by a preparative scale bulk electrolysis coupled to product analysis and isolation, to determine the efficiency of the conversion.

2
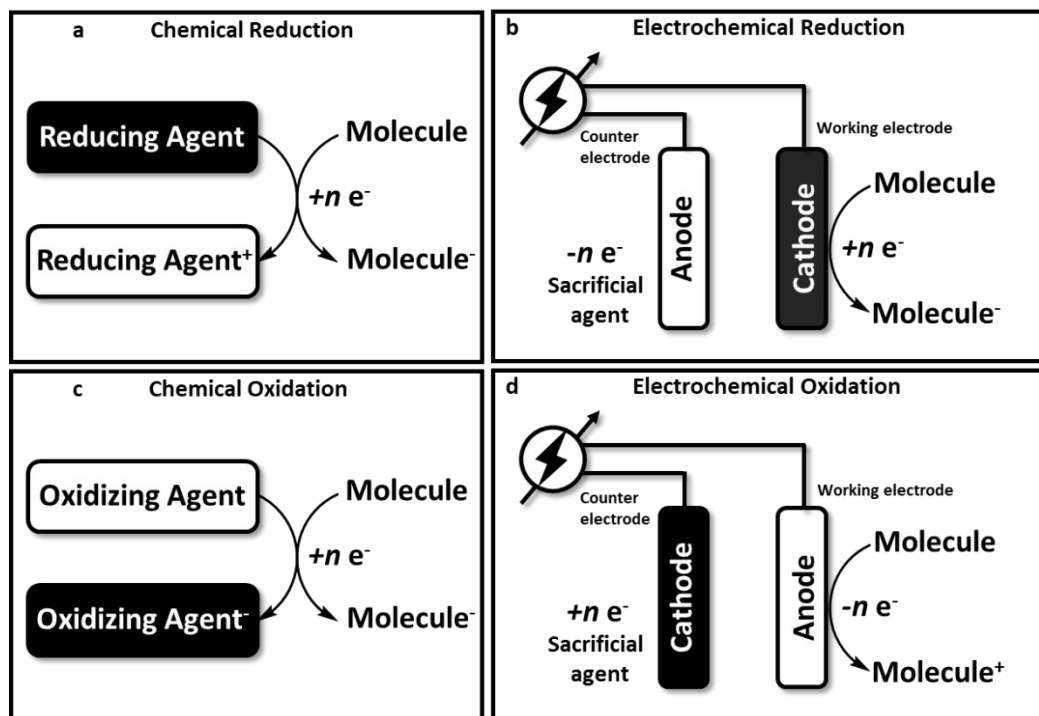
Figure 2. Chemical vs electrochemical oxidation and reduction reactions. a. generic chemical reduction. b. electrochemical reduction. c. generic chemical oxidation. d. electrochemical oxidation reaction.

As mentioned previously, the replacement of chemical reducing (Figure 2a) or oxidizing agents (Figure 2c) with cathodes (Figure 2b) and anodes (Figure 2d), respectively, has a positive impact on the overall safety of the chemical process. Several of the common strong reducing and oxidizing agents have extensive handling, use and disposal precautions listed in their materials safety datasheets and require training to use.

Let's next look at an example of a standard chemical reduction reaction. In a reduction reaction, a molecule receives an electron from a chemical species (the reducing agent), which in turn becomes oxidized (Figure 2a). An analogous electrochemical process replaces the reducing agent with a cathode (Figure 2b). The cathode then delivers the electrons to the molecule to be reduced. To account for all the charge passed, however, the anode of the experiment will need to remove electrons from the system. For this to occur, a sacrificial redox couple is usually employed. Additionally, a separator may be used to ensure that the species in the cathodic chamber are isolated from the anodic side of the cell. Akin to the side-by-side comparison in 2a and 2b, a chemical oxidation process can be translated into an electrochemical step. Instead of using the chemical oxidizer to remove an electron from the molecule of interest (Figure 2c), the anode in the experiment removes the electrons instead (Figure 2d). The cathode in this experiment delivers the necessary charge to maintain neutrality to a sacrificial agent to be reduced. The electrode where the desired chemistry is occurring is additionally referred to as the working electrode, whereas the electrode that is used to maintain charge neutrality is dubbed the counter electrode, because it provides the counter charge.

Conventions. Several conventions are utilized in electrochemical measurements. For the purposes of this paper, we use positive current and voltage as corresponding to oxidation/anodic processes, with negative current and voltage pertaining to cathodic reactions.

Conversion of potentials and reference electrodes. With a mature science of electrochemistry also comes a wide variety of ways to measure potential and currents. In controlled potential experiments, the potential

is measured against a reference, which does not change over time.[1] Some common references stable in aqueous media across a wide pH range are the saturated calomel electrodes (SCE) which stands at 254 mV vs the normal hydrogen electrode (NHE) and silver/silver chloride Ag/AgCl at 200 mV vs NHE. A reference that is stable and commonly utilized in organic media is the ferrocene/ferrocenium redox couple, Fc/Fc^+ at 590 mV vs NHE. For the purposes of a common scale, all potentials in this paper are reported vs Fc/Fc^+ to facilitate side-by-side comparisons.

Metrics: In the field of homogeneous catalysis, number of turnovers and turnover frequencies (turnovers per unit time) are common metrics of relative activities. Through the lens of a mediated electrochemical process, such metrics still apply when the mediator, or catalyst is driven by either electrical current or potential. However, an additional type of metrics become relevant when considering electrode-driven processes at catalytically active surfaces: electrochemically active surface areas and consequently current densities measured in units of current per surface area.[5] A higher catalytically active surface area has more active sites. Additionally, a higher current density can in principle enable a higher rate of chemical conversion per unit time. In fact, relative catalytic activity for electrochemical reactions in the field of solar fuel synthesis is defined as the overpotential necessary to achieve a 10 mA cm^{-2} sustained current density during bulk electrolysis.[6] Comparisons of catalytic activity based on these parameters require good Faradaic efficiencies and an accurate way to measure the active surface area of the electrode.

The present review acknowledges these important catalytic metrics but points out that such elements have not permeated the field of mediated electrochemical synthesis. For the purposes of our discussion, we focus on descriptive molecular aspects of mediated electrochemical transformations. While the nature of the electrodes chosen and their size may play a role in the chemistries observed, further studies are necessary to produce experimental evidence for the discrete chemical steps at surfaces.

With this knowledge in mind, we now begin to describe recent one-electron chemistries that have been utilized to construct bonds to C through radical mechanisms (Figure 3). Recent advances have shown that radicals can be generated by mediated reduction (blue) or mediated oxidation (orange red). Carbon dioxide, carbon halogen bonds and even nitriles can be electrochemically or photoelectrochemically reduced by strong reducing reagents generated at electrodes. Potent electrode-generated oxidants can also be used to trigger the formation of radicals across a variety of functional groups such as carbons alpha to a nitrogen, carboxylates, trifluoroborate salts (RBF_3K), carbon halogen bonds and even C-H bonds.
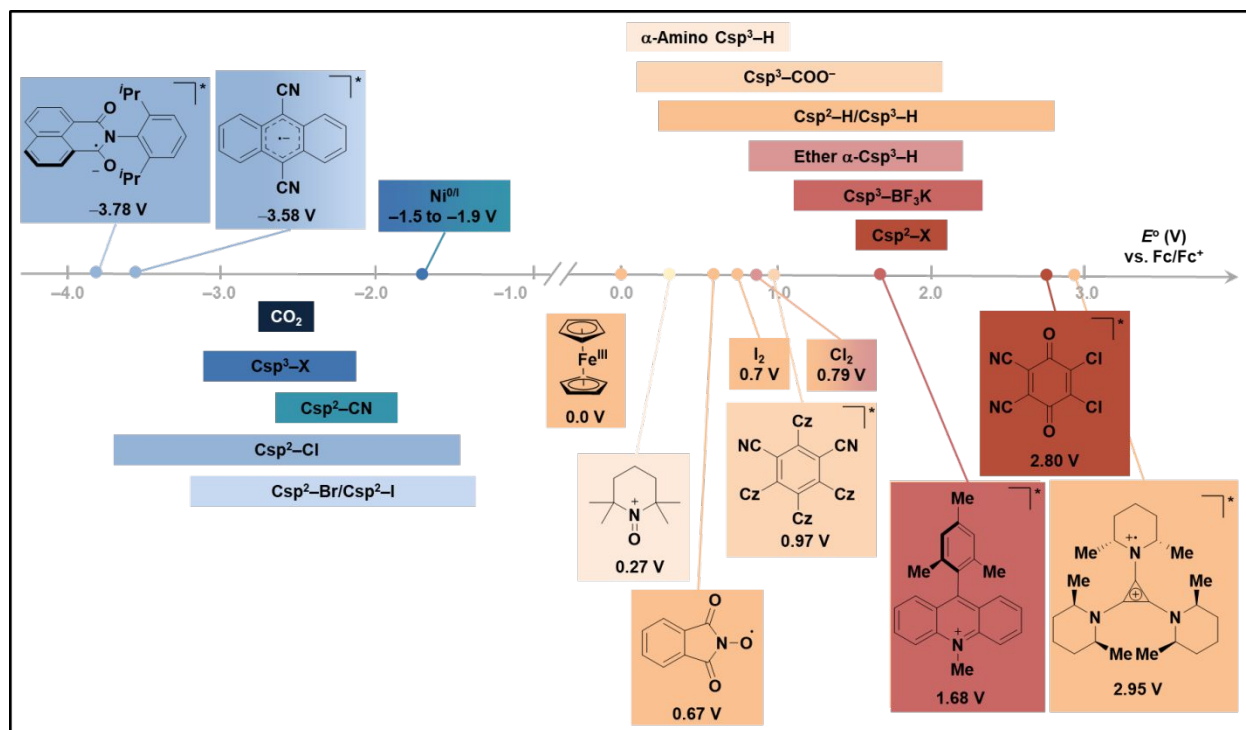
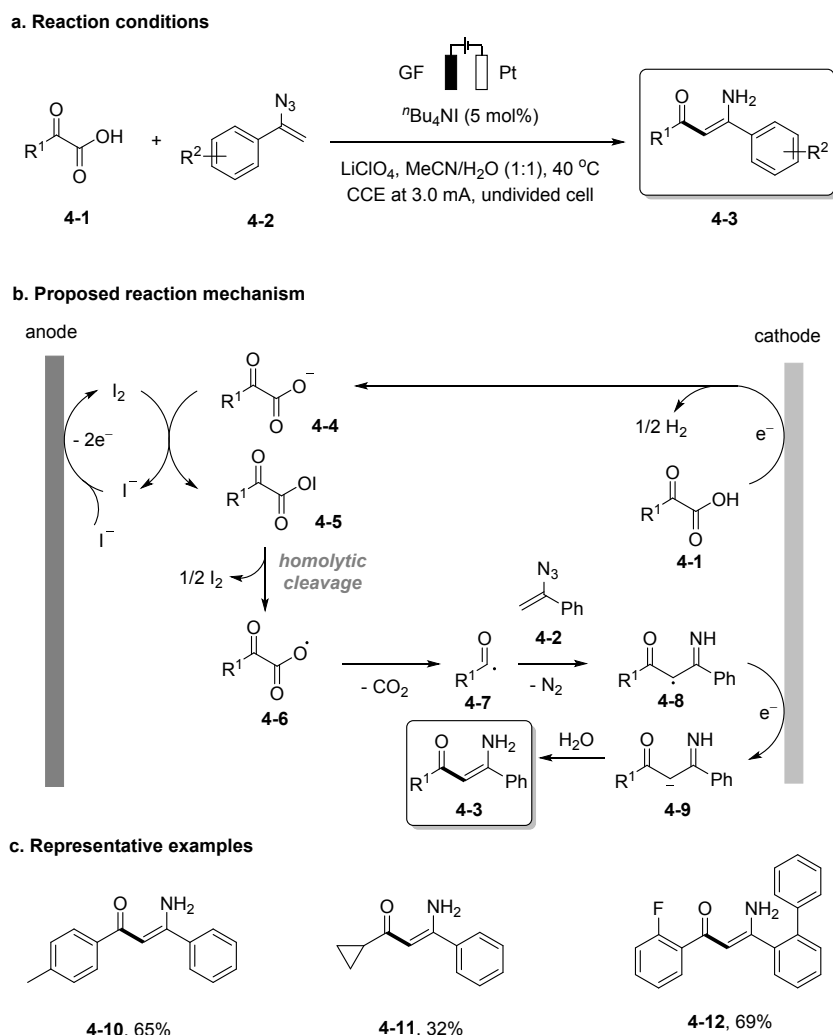**Figure 3.** Potential matching for mediators and reaction substrates in this review.

2. C–C bond coupling reactions

C–C bond formation via radical mechanisms enabled by electrochemistry has been heavily investigated over the past two decades, in part due to the extensive use of cross coupling reactions in pharmaceutical synthesis.[7, 8] From Kolbe's 1848 work, numerous synthetic methodologies from direct electrolysis to electrocatalysis have been realized to selectively generate the reactive carbon-centered radical species, which are further oxidized or trapped by various reagents to forge new bonds to carbon.[9] In the following sections, we summarize the recent advances in electrochemical and electrophotochemical C–C bond-forming reactions that involve C-radical intermediates.

2.1. Mediated C-C bond formation at anodes

2.1.1. C–C decarboxylation

The homolytic cleavage of weak heteroatom-halogen bonds is a powerful approach for the generation of reactive radical species that further react to form carbon-heteroatom bonds. In 2019, Kong et al reported an electrochemical approach to synthesize unprotected enaminones from decarboxylative coupling between α-keto acids and organic azides (Figure 4).[10] For this C–C bond deconstructive functionalization method, iodide salt was used as a redox mediator. Interestingly, control experiments and CVs revealed that the conjugated base **4-4** is the active intermediate, which would react with the anodically generated molecular iodine to form the hypoiodite **4-5**.[10, 11] A catalytic current increase for $I^-/I_3^-/I_2$ redox couples by addition of a carboxylate salt was also observed by Wang et al in a related Minisci-type acylation of N-heteroarenes.[11] Upon homolytic dissociation of the O–I bond, radical **4-6** is generated and undergoes decarboxylation to form the acyl radical **4-7**. Further trapping of **4-7** by vinyl azide **4-2** with nitrogen extrusion leads to the formation of intermediate **4-8**, which undergoes cathodic reduction followed by protonation to form the enaminone product. The key intermediate anion **4-4** is formed through proton reduction on the cathode.

a. Reaction conditions

b. Proposed reaction mechanism

c. Representative examples

**4-10**, 65%   **4-11**, 32%   **4-12**, 69%

Figure 4. Electrochemical enaminone formation mediated by iodide. GF = graphite felt. a. reaction conditions for enaminone formation b. proposed reaction mechanism c. representative examples. [10]

In 2019, Lin and Huang developed a method for electrochemical C3-formylation of indoles with glyoxylic acid as a C_1 synthon.[12] The presence of catalytic loading of a primary or secondary amine facilitates the decarboxylation of glyoxylic acid through an α-iminium carboxylate intermediate. An analogous intermediate was also previously observed.[13] Under the standard reaction conditions, a broad variety of *N*-protected and unprotected indoles reacted smoothly to form the formylated products (Figure 5). The reaction is initiated by an imine condensation to form intermediate **5-7**, which undergoes deprotonation with a loss of hydrogen on the cathode to form the reactive species **5-4**. CV experiments showed that the peak potential for the irreversible oxidation of the corresponding α-iminium carboxylate **5-6** is about 0.62 V lower than the potential necessary for the oxidation of glyoxylic acid.[12] Subsequent anodic oxidation and decarboxylation of **5-4** delivers radical cation species **5-5**. Rapid anodic oxidation of **5-5**, followed by a nucleophilic attack by indole, generates intermediate **5-6**. Further hydrolysis of **5-6** yields the product and regenerates the amine catalyst. Thoughout the whole process, the amine organocatalyst promotes both the electrochemical decarboxylation and the nucleophilic reaction.
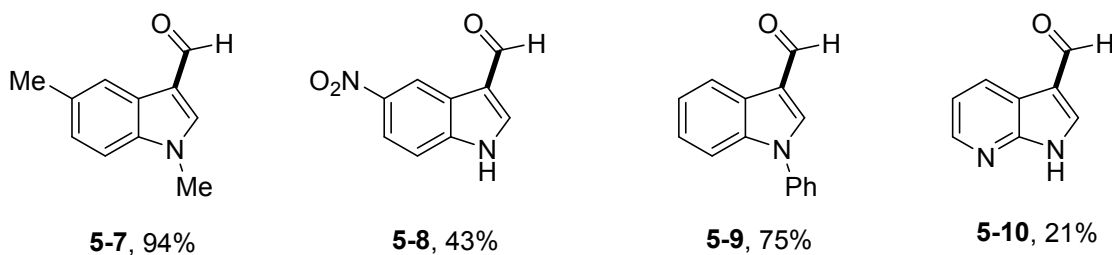
a. Reaction conditions

b. Proposed reaction mechanism

c. Representative examples

5-7, 94%   **5-8**, 43%   **5-9**, 75%   **5-10**, 21%
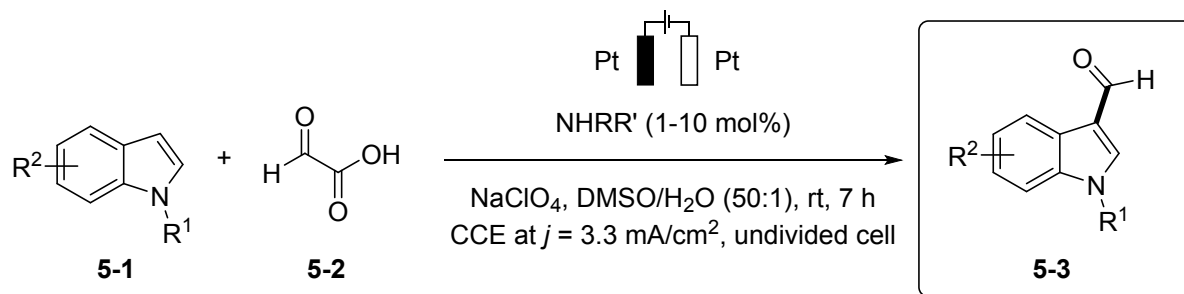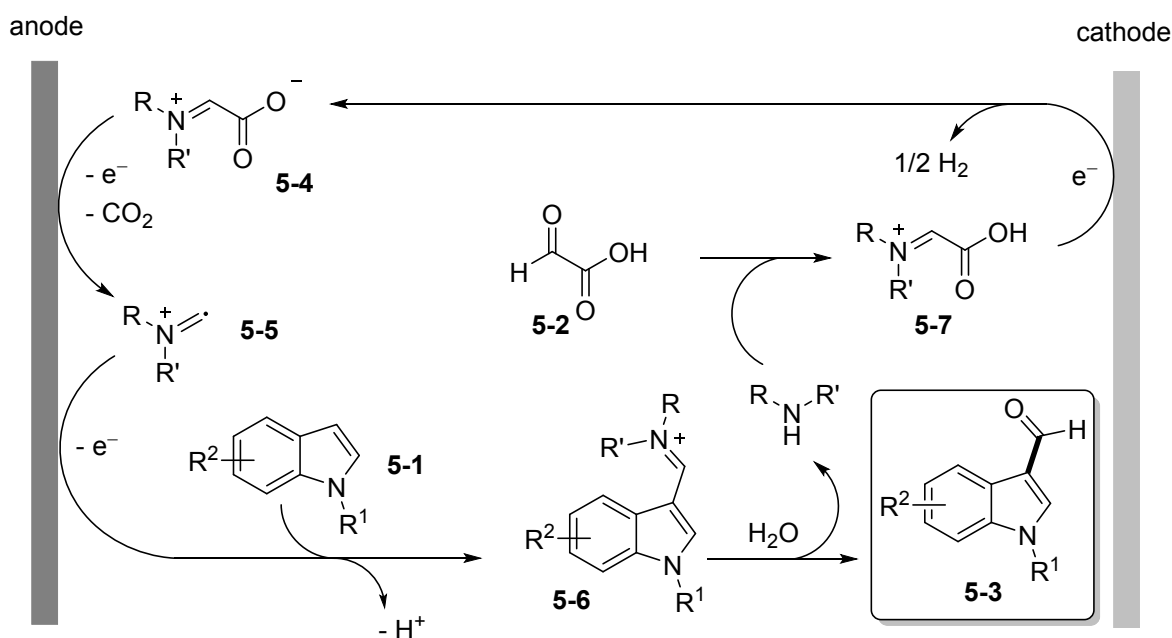
Figure 5. Electrochemical C3-formylation of indole with glyoxylic acid; a. reaction conditions b. proposed reaction mechanism c. representative examples. [12]

In 2020, Lai et al reported electrophotochemical approaches for the alkylation of *N*-heteroarenes with aliphatic carboxylic acids.[14] The relatively inexpensive $CeCl_3 \cdot 7H_2O$ was proved to be an efficient photocatalyst under acidic conditions, to promote both the decarboxylation of carboxylic acids and to activate the *N*-heteroaromatic substrates. For this decoupled electrophotocatalysis, the oxidizing Ce^{IV} intermediate **6-6** is produced by anodic oxidation and coordinates a carboxylate anion to form the complex

**6-7**. This complex then undergoes photo-induced ligand-to-metal charge transfer to afford a carboxyl radical and regenerate the Ce^{III} **6-8** species back to the catalytic cycle. Upon decarboxylation of the carboxyl radical **6-9**, the generated alkyl radical **6-10** is then trapped by a protonated pyridine to form **6-11**. Further oxidation, mediated by the Ce^{IV}/Ce^{III} redox couple, and deprotonation of this transient species **6-11** generates the alkylated product **6-3**. This example demonstrates an efficient decarboxylative C–H bond functionalization strategy through a combination of photo-induced radical formation with electrode driven catalyst regeneration. The proposal of a mechanism that involves an alkyl radical species is supported by radical clock experiments.[14]

The authors also extended the reaction scope to electrophotochemical carbamoylation of heteroaromatics with oxamic acids. The photocatalyst 4CzIPN (2,4,5,6-tetrakis(9H-carbazol-9-yl)isophthalonitrile) was employed as the redox mediator for the oxidation of oxamic acids (Figure 6). The excited species 4CzIPN* ($E_{p/2}^{red}$ = 0.97 V vs Fc/Fc^{+}) undergoes thermodynamically favorable single-electron transfer (SET) with an oxamic acid molecule to generate the carbamoyl radical **6-15**. Decarboxylation of **6-15**, followed by trapping with a protonated pyridine, affords the radical cation **6-17**. The observation of a dihydroquinoline intermediate during the electrolysis of an analogous quinoline suggests that **6-17** further accepts an electron from the persistent and highly reducing **6-14** to afford intermediate **6-18**. Ultimately, 2-electron oxidation of the stable species **6-18** produces the carbamoylated product. Hydrogen evolution from the cathodic side compensates for the electrons transferred to the anodic surface.
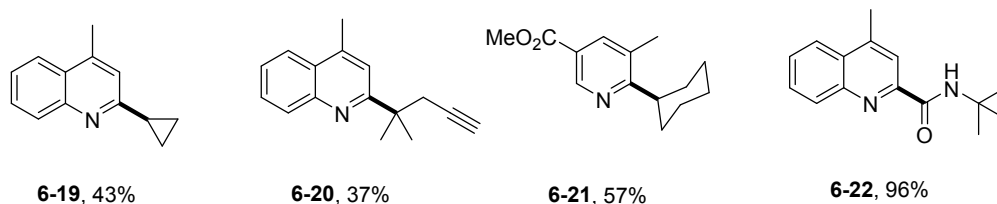
a. Reaction conditions
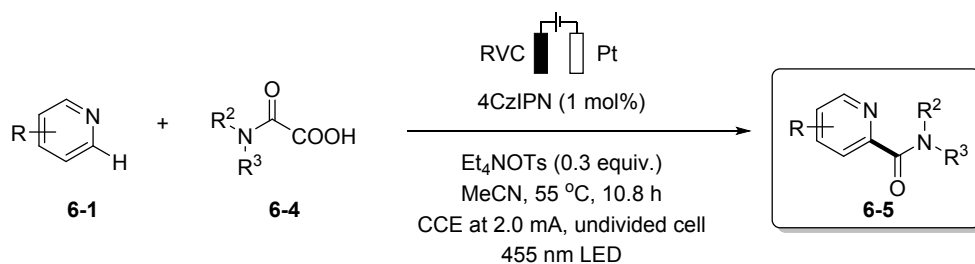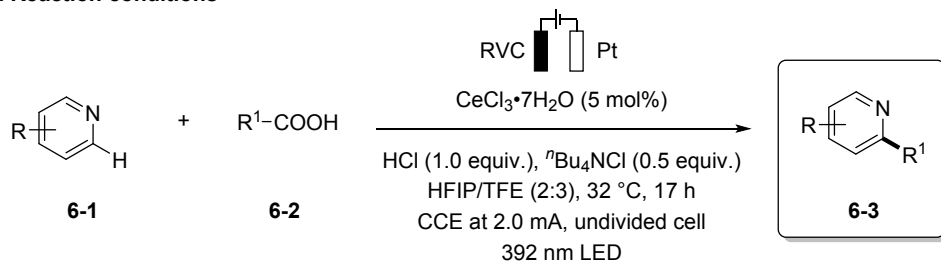
b. Proposed reaction mechanism

c. Representative examples

6-19, 43%   6-20, 37%   6-21, 57%   6-22, 96%
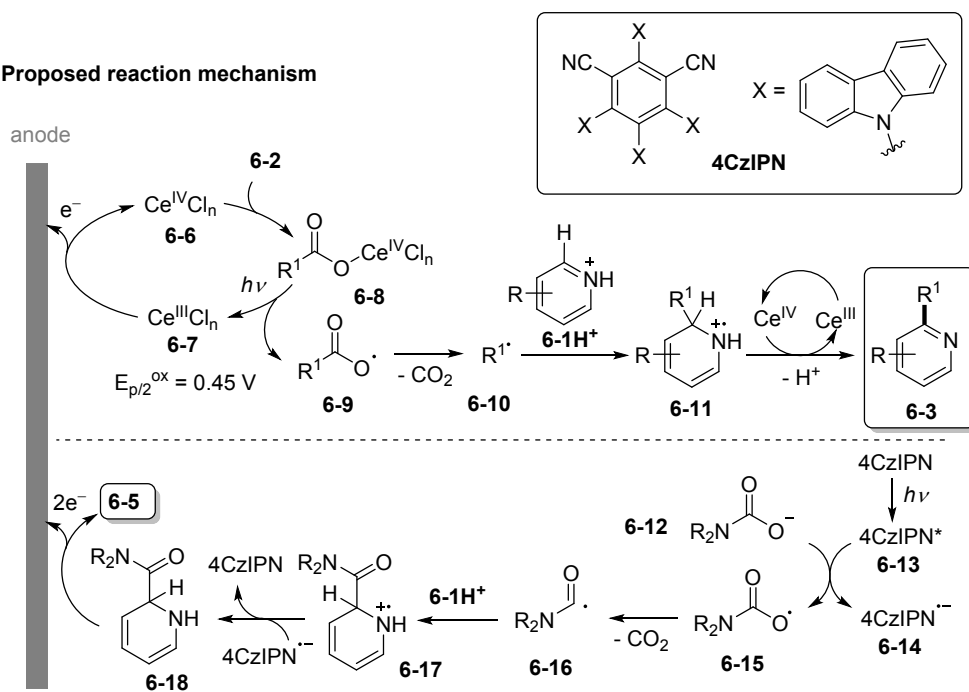
Figure 6. Electrophotocatalysis for alkylation and carbamoylation through oxidative decarboxylation of carboxylic and oxamic acids. RVC = reticulated vitreous carbon. HFIP = 1,1,1,3,3,3-hexafluoroisopropanol. TFE = 2,2,2-trifluoroethanol. 4CzIPN = 2,4,5,6-tetrakis(9H-carbazol-9-
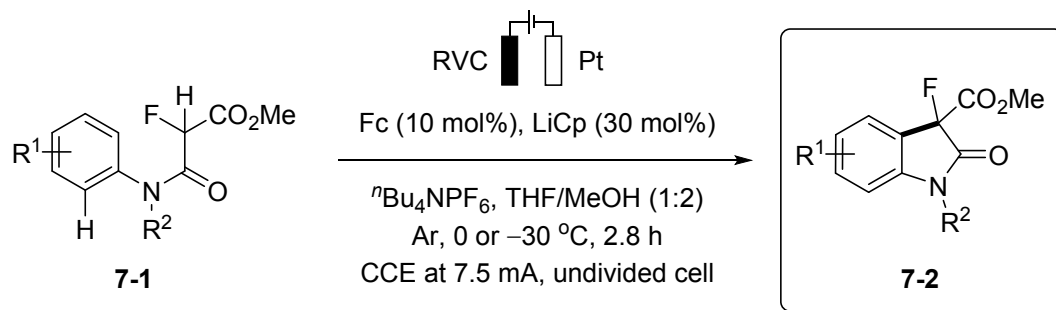
yl)isophthalonitrile; a. reaction conditions for enaminone formation b. proposed reaction mechanism c. representative examples.[14]

2.1.2. C–H bond activation

α-Csp³–H activation of carbonyl compounds

In 2017, Wu and Xu reported a carbon radical-involved intramolecular cross-coupling between Csp^2–H and Csp^3–H bonds. They utilized the reaction to synthesize C3-fluorinated oxindoles under mild electrocatalytic conditions.[15] Ferrocene (Fc) was employed as an oxidative mediator for the oxidation and C–H activation of the starting fluorinated malonate amides (Figure 7). For CV experiments, a catalytic current was observed for the oxidation of Fc in the presence of substrate **7-1** and LiOMe as the base, while no electron transfer was observed between Fc^+ and the starting material **7-1** due to a large potential difference of 1.41 V between the redox signatures of the two species. Mechanistically, the key anionic intermediate **7-3** was formed by deprotonation by added LiCp or MeO^- (generated upon cathodic reduction of MeOH). Though this deprotonation step is thermodynamically unfavorable, the driving force for the process is the facile electron abstraction by Fc^+ and oxidation of **7-3** to form the carbon radical **7-4**. Sequential radical cyclization and oxidative re-aromatization produces the final oxindole **7-2**. This mild electrocatalytic cyclization method allows access to a broad variety of C3-fluorinated oxindoles bearing halogen, protected alcohol, and protected amine functional groups in good to excellent yields.
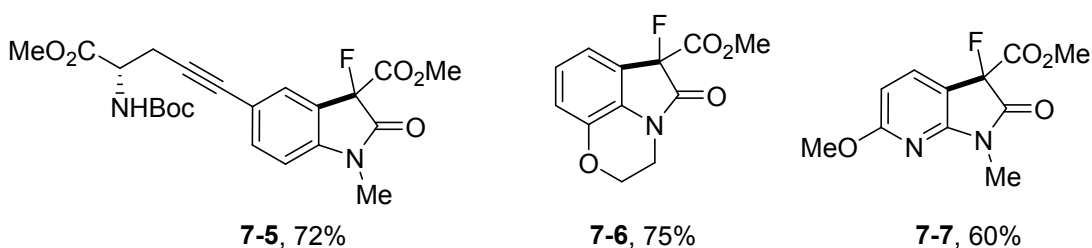
a. Reaction conditions

**b. Proposed reaction mechanism**

c. Representative examples

**7-5**, 72%   **7-6**, 75%   **7-7**, 60%
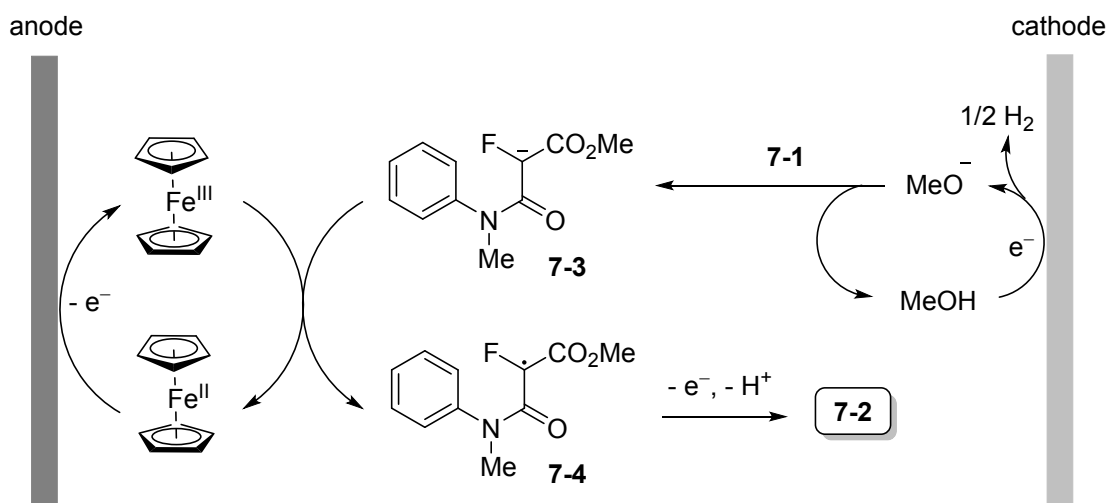
Figure 7. Intramolecular cyclization to synthesize C3-fluorinated oxindoles with ferrocene as redox mediator. RVC = reticulated vitreous carbon. a. reaction conditions for enaminone formation b. proposed reaction mechanism c. representative examples. [15]

A follow-up study reported the intramolecular assembly of oxindole derivatives using Fc as an electrocatalyst and Y(OTf)$_3$ as a Lewis acid additive (Figure 8).[16] The presence of a strong base like LiOMe is essential for the activation of the substrate. Noteworthily, substrates bearing acidic α-alkyl malonic ester moieties are reactive without the need for a Lewis acid additive or a strong base. Substrate **8-3** can react smoothly under optimized conditions to produce 3,4-dihydro-1*H*-quinolin-2-one derivatives **8-4** in good to excellent yields.
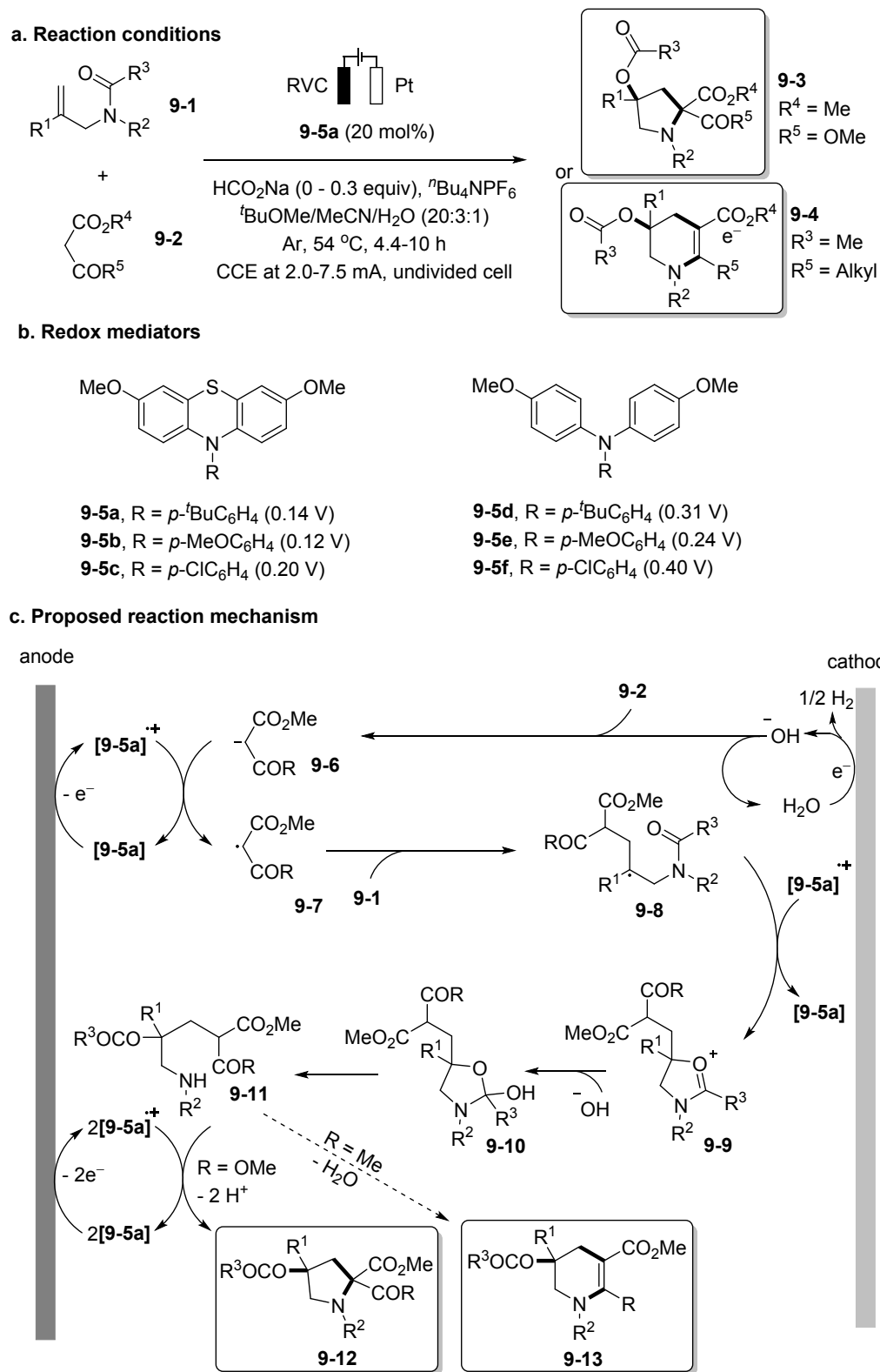
a. Reaction conditions

b. Representative examples

8-5, 85%   **8-6**, 67%   **8-7**, 88%   **8-8**, 96%
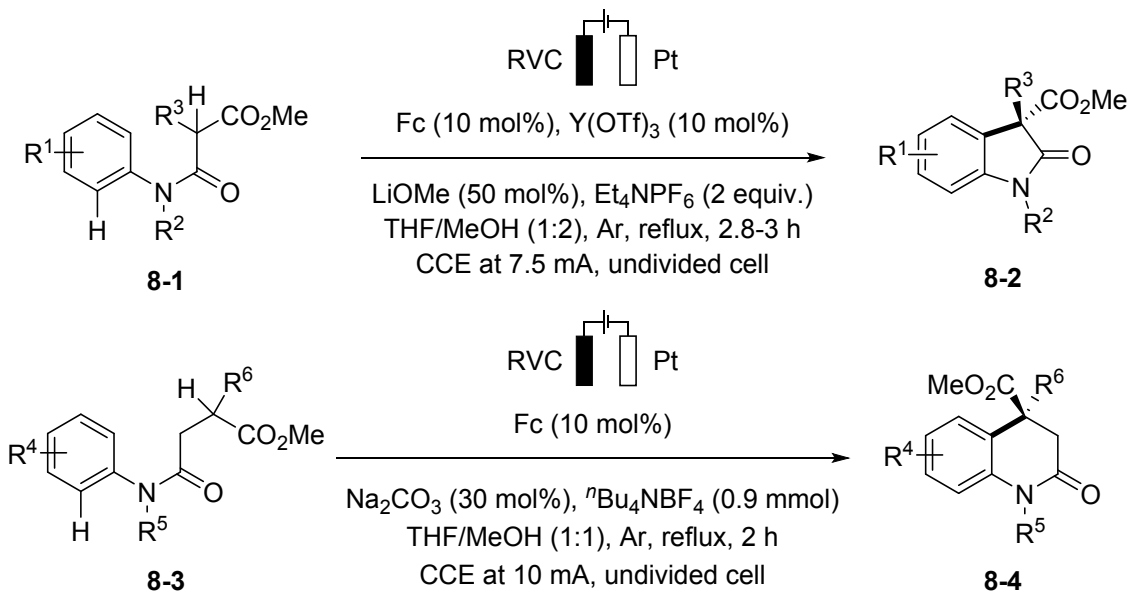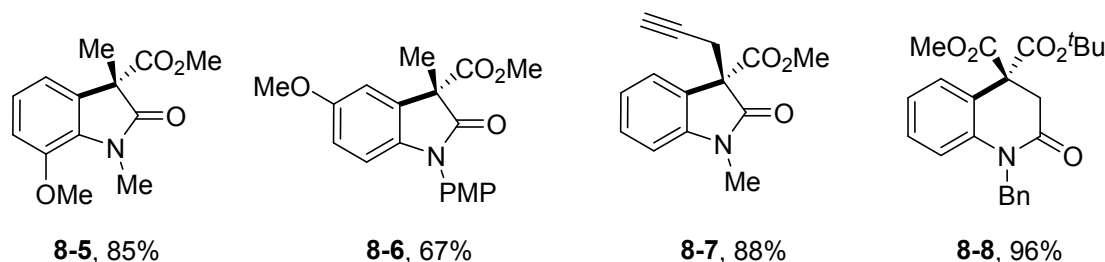
Figure 8. Ferrocene-electrocatalyzed intramolecular Csp^2-Csp^3 coupling reaction. RVC = reticulated vitreous carbon. PMP = *para*-methoxyphenyl; a. reaction conditions for enaminone formation b. representative examples. [16]

Taking advantage of the 1,3-dicarbonyl functionality as precursor to electrophilic C-radicals,[17] Xu and co-workers developed a method for cascade dehydrogenative annulation of 1,3-dicarbonyl compounds with *N*-allyl amide to synthesize 5- and 6-membered *N*-heterocycles.[18] Phenothiazine derivatives were used as electrocatalysts for the transformation, which showcased better reactivity compared to analogous triarylamines (Figure 9). CV experiments revealed that direct electrolysis of both substrates is not feasible due to their high oxidation potentials. Additionally, the sodium formate additive was unable to promote the oxidation of 1,3-dicarbonyls. Instead, the substrate **9-2** is deprotonated by hydroxide, generated via cathodic water reduction, to form the anionic species **9-6** ($E_{p/2}$ = –0.07 V vs Fc/Fc$^+$, R = OMe). Thermodynamically favorable electron transfer between the oxidized phenothiazine **[9-5a]**$^{+\bullet}$ ($E_{p/2}^{red}$ = 0.14 V vs Fc/Fc$^+$) and **9-6** generates the C-radical **9-7**. Trapping of this radical species by the alkenyl moiety of the N-allyl amide substrate, followed by another loss of electron delivers the intermediate **9-9**. A nucleophilic attack by OH$^-$ or H$_2$O affords **9-10**, which undergoes a selective C–N bond cleavage to produce the secondary amine intermediate **9-11**. In case of malonic esters (R = OMe), two proton-coupled electron transfer (PCET) events occurred to form the pyrrolidine product **9-12**, as supported by observations of catalytic current in CV experiments.[18] Alternatively, the tetrahydropyridine product **9-13** can be formed upon intramolecular dehydration of amine **9-11** in the case of β-keto esters (R = Me).
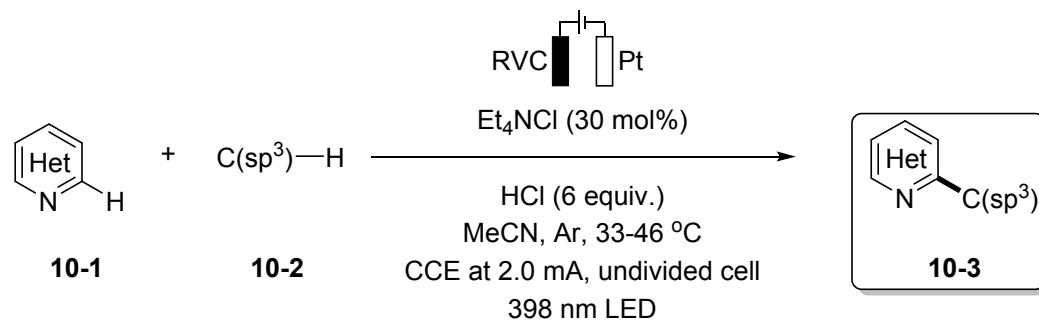
12

Figure 9. Phenothiazine-mediated electrochemical annulation of *N*-allyl amides with 1,3-dicarbonyl compounds. The numbers in the parentheses are the anodic half-peak potentials (vs Fc/Fc$^+$); a. reaction conditions for enaminone formation b. redox mediators c. mechanism. [18]

13

Activation of cycloalkanes and heteroatom-adjacent Csp³–H bonds

Cross-dehydrogenative coupling reactions are among the most powerful strategies for forging new C–C bonds. This type of coupling has a high atom economy and the wide availability of starting materials renders it especially useful. In this context, there has been significant interest in developing new methods for radical coupling between aliphatic C–H bonds and heteroarenes (Figure 10).[19] However, the generation of reactive radical intermediates from alkanes and other heteroatom-adjacent Csp³–H bonds is difficult. This challenge is due to their inherently high bond dissociation energies (BDE). General methods for the generation of radical intermediates from aliphatic C–H bonds employ the use of chemical oxidants such as peroxide, persulfate, hypervalent iodine, or Selectfluor.[20-22] However, the use of stoichiometric chemical radical initiators limits their application in large-scale synthesis and lower the atom economy of the whole process.[23] In 2020, Xu et al addressed this challenge in aliphatic C–H bond activation by electrophotocatalysis.[24] In this chemistry, chlorine radicals are produced in situ by anodic oxidation of chloride salts followed by light-induced Cl–Cl bond homolysis. These radicals act as a hydrogen atom transfer (HAT) catalyst to abstract hydrogen atoms from a broad variety of C–H bonds to form alkyl radicals. The driving force for the process lies in the relatively large BDE of HCl (102 kcal mol^{-1}) compared to most unactivated aliphatic C–H bonds in cycloalkanes, methylarenes, ethers, and amides. The resulting radicals can then add to a protonated N-heteroarene to furnish the C2- or C4-alkylated pyridine products through a Minisci-type mechanism (Figure 10b). In this process, the reactive chlorine radical can also act as an oxidant for the rearomatization of intermediate **10-5**.
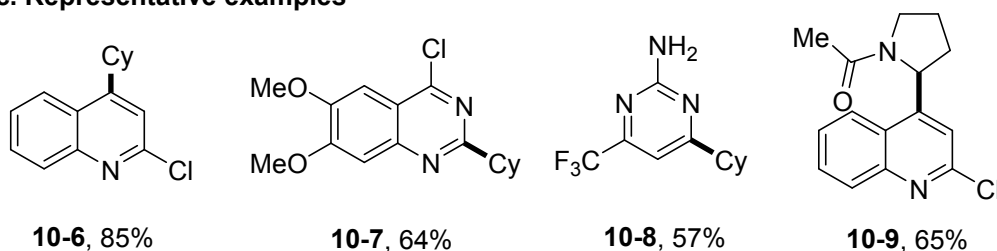
a. Reaction conditions

b. Proposed reaction mechanism

c. Representative examples

10-6, 85%   **10-7**, 64%   **10-8**, 57%   **10-9**, 65%
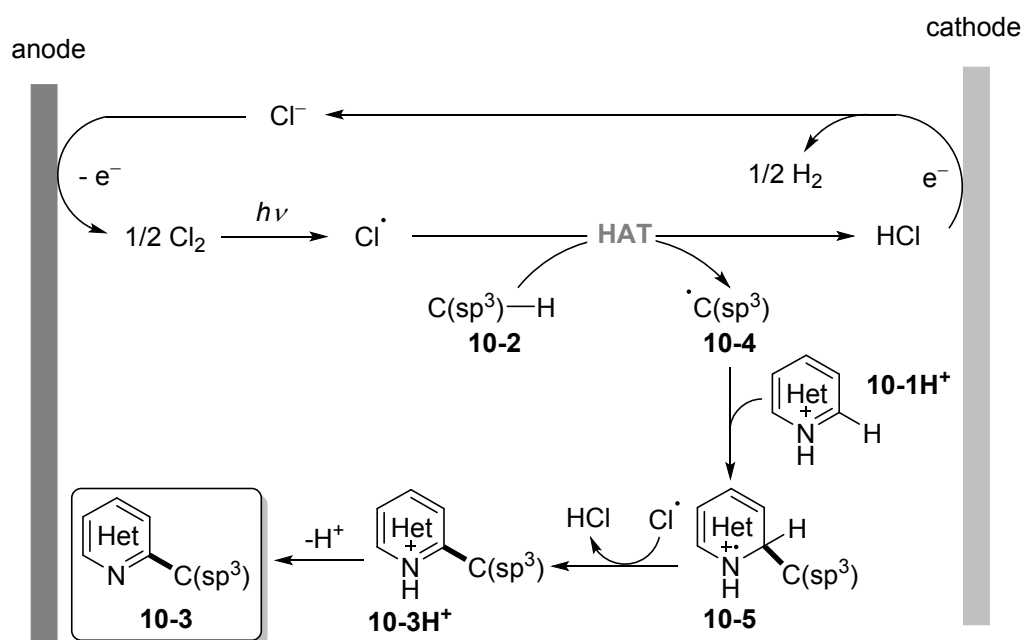
Figure 10. Chloride-mediated electrophotochemical alkylation of *N*-heteroarene. RVC = reticulated vitreous carbon; a. reaction conditions for enaminone formation b. proposed reaction mechanism c. representative examples. [19]

In separate work, Lambert and co-workers developed a method for direct C–H functionalization of ethers with a triaminocyclopropenium cation (TAC[+]) as an electrophotocatalyst (Figure 11).[25] Mechanistically, the chemistry was driven by the oxidation of TAC[+] at the anode to form the radical dication TAC[•2+] (E =

0.88 V vs Fc/Fc$^+$), followed by visible light photoexcitation to afford the highly oxidizing excited species [TAC$^{\bullet 2+}$]* (E ≈ 2.95 V vs Fc/Fc$^+$). The excited radical dication [TAC$^{\bullet 2+}$]* reacts with ether to produce an α-alkyl radical through a hydrogen atom transfer. This reaction regenerates TAC$^+$ back to the electrophotocatalytic cycle. Further trapping of the radical **11-4** with quinolines, electron-deficient alkenes, or azoles produces the Minisci-type C2-alkylated quinolines, hydroalkylated alkenes, or N-alkylated heteroaromatic products. It should be noted that the ether functionalization by direct electrolysis can be challenging since the radical intermediate **11-4**, formed upon 1-electron oxidation of ether, is more easily oxidized than the ether itself. Therefore, the anode provides the capacity for multiple sequential oxidation events that can lead to undesired side-reactions. In contrast, the electrophotocatalytic approach maintains only a minute concentration of active oxidant and leads to productive 1-electron chemistry.[25]
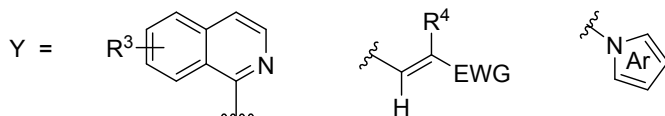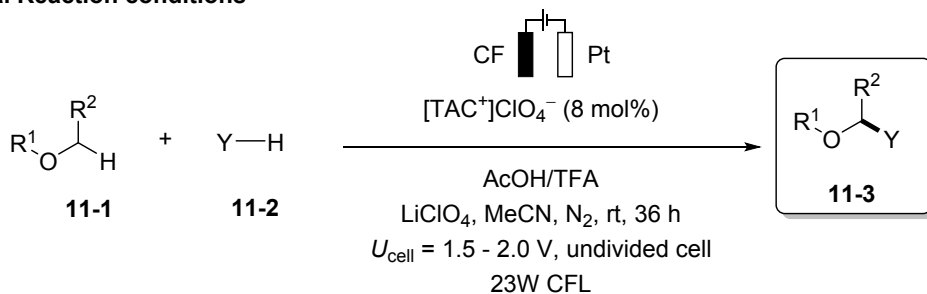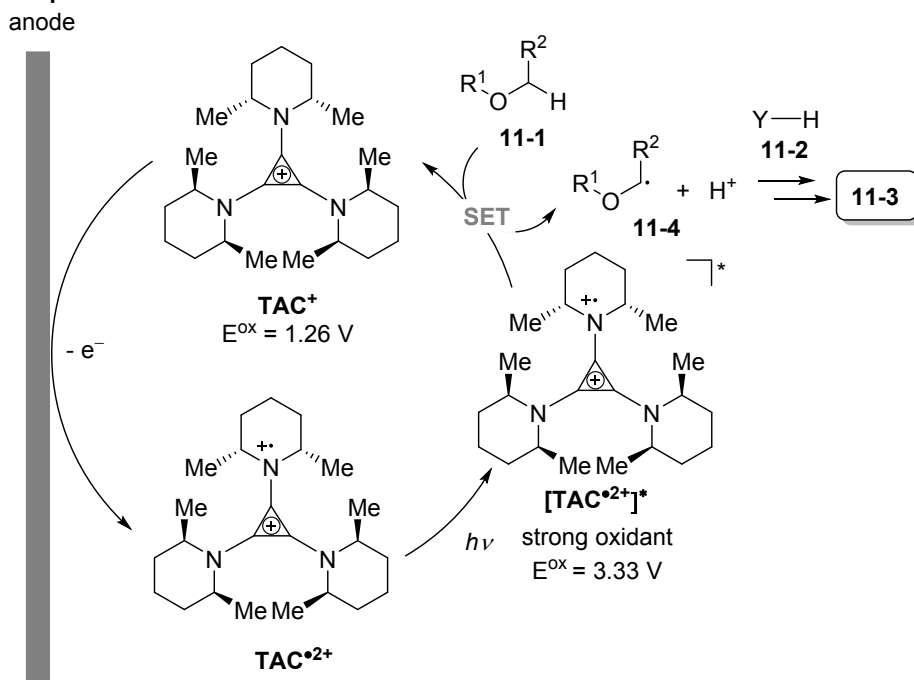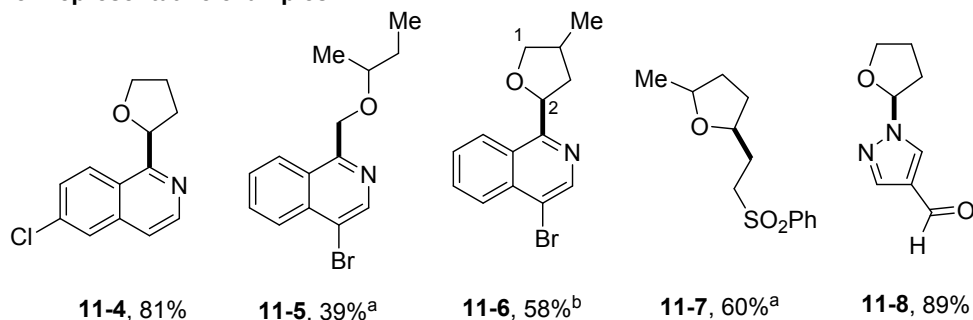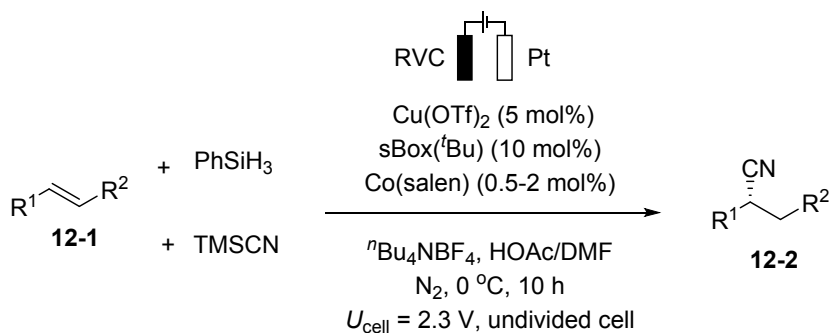
Figure 11. TAC[+]-mediated cross-dehydrogenative coupling between *N*-heteroarenes and ethers. CF = carbon felt. TFA = trifluoroacetic acid. [a] One regioiosmer formed. [b] C1 : C2 = 1.2 : 1.4.; a. reaction conditions b. proposed reaction mechanism c. representative examples. [25]

17

Alkenes and alkynes functionalization

In 2020, Song et al demonstrated two radical reactions in tandem– Co-mediated HAT and Cu-mediated radical cyanation – to enable highly enantioselective hydrocyanation of conjugated alkenes (Figure 12).[26] For this dual electrocatalytic approach, reactive Co^{III}–H and Cu^{III}-CN complexes are generated by anodic oxidation simultaneously. Mechanistically, the alkene substrate is first activated by Co^{III}–H through HAT to deliver the radical species **12-6**, which undergoes cyanation by another equivalent of Cu^{III}-CN to produce **12-2**. The enantioselectivity of this approach was accomplished using chiral sBox(^{t}Bu) ligand (Figure 12b), which coordinates with copper to form a chiral complex. Based upon density functional theory (DFT) calculations, the pendant ester group on the chiral ligand played a key role in enhancing the stereoselectivity of the reaction via a C–H$\cdots\pi$ interaction with the aryl moiety of the alkene substrate.
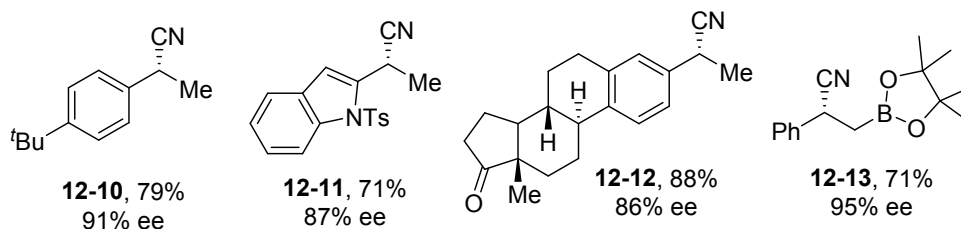
a. Reaction conditions

b. Proposed reaction mechanism

c. Representative examples

12-10, 79%
91% ee

12-11, 71%
87% ee

12-12, 88%
86% ee

12-13, 71%
95% ee
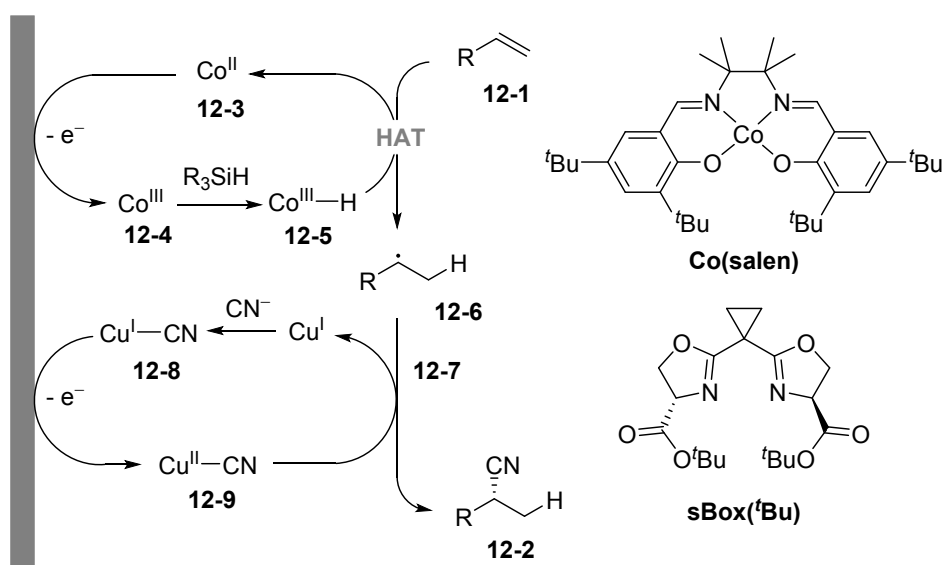
Figure 12. Copper and cobalt co-catalyzed electrochemical hydrocyanation of alkenes. RVC = reticulated vitreous carbon; a. reaction conditions b. proposed reaction mechanism c. representative examples. [26]

In 2018, Ye et al combined two distinct anodic events for selective functionalization of alkenes (Figure 13).[27] In this anodically coupled electrolysis, the pairing of the two radical precursors with a metal catalyst was carefully controlled to achieve high chemoselectivity and regioselectivity of the products. Langlois's reagent CF_3SO_2Na ($E_{p/2}$ = 0.8 V vs Fc/Fc$^+$) was chosen as the CF_3 radical source, while [Mn^{III}–Cl] serves as the chlorine radical source with $E_{1/2}$ (Mn^{II}/Mn^{III}) = 0.78 V vs Fc/Fc$^+$. The [Mn^{III}–Cl]/ [Mn^{II}–Cl] redox couple showed a pair of reversible redox waves, indicating the lifetime of the latent Cl radical **13-9** is

comparable to the timescale of CV experiments. In the proposed mechanism, the alkene substrate is first activated by the addition of CF_3 radical, which is formed by 1-electron anodic oxidation of CF_3SO_2Na salt, to form the intermediate **13-6**. The highly persistent [Mn^{III}–Cl] species then transfers a chlorine atom to **13-6** to yield the product and regenerate a Mn^{II} species back to the $Mn^{II/III}$ cycle. The mechanism and the order of radical addition are supported by radical clock experiments (Figure 13c). The method was also applied for the synthesis of chlorotrifluoromethylated pyrrolidines via radical ene-yne cyclization in a separate work (Figure 14).[28] The alkene Z/E stereoselectivity in product formation was driven by the geometry of the intermediate **14-3**.
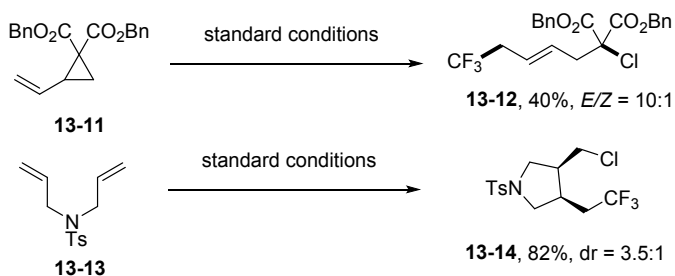
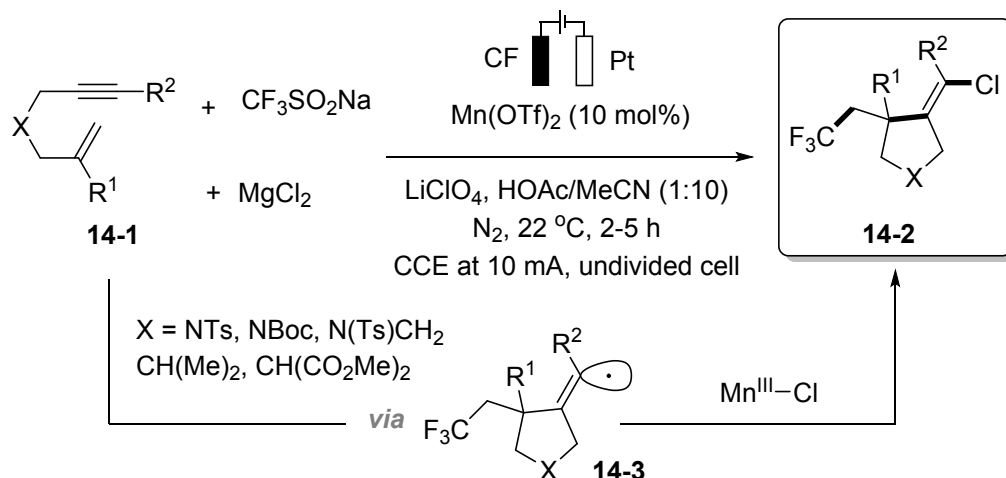**a. Reaction conditions**
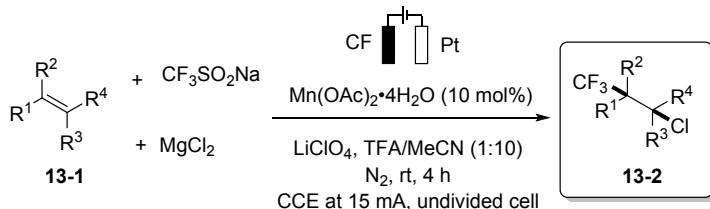
b. Proposed reaction mechanism
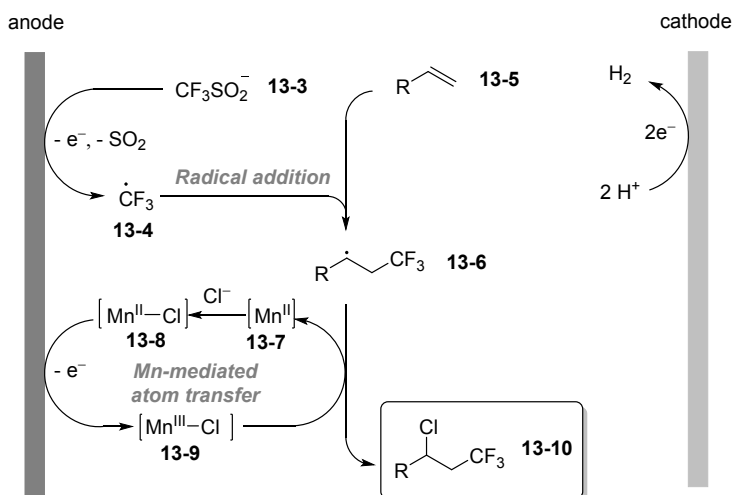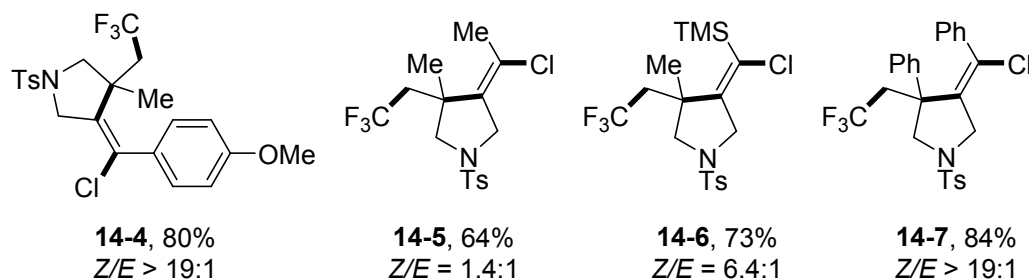
c. Radical clock experiments

Figure 13. Anodically coupled electrocatalytic difunctionalization of alkenes. CF = carbon felt. TFA = trifluoroacetic acid. a. reaction conditions b. proposed reaction mechanism c. radical clocks. [27]

a. Reaction conditions

b. Representative examples

14-4, 80%   **14-5**, 64%   **14-6**, 73%   **14-7**, 84%
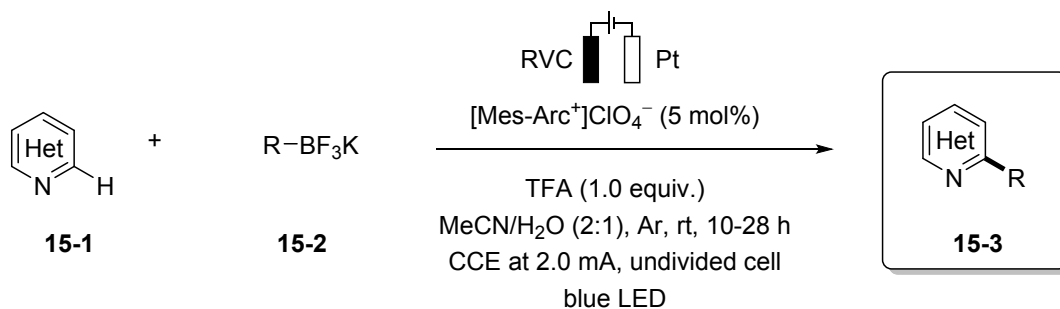*Z/E* > 19:1   *Z/E* = 1.4:1   *Z/E* = 6.4:1   *Z/E* > 19:1

Figure 14. Synthesis of chlorotrifluoromethylated pyrrolidines by electrocatalytic radical ene-yne cyclization. CF = carbon felt. a. reaction conditions b. representative examples.[28]
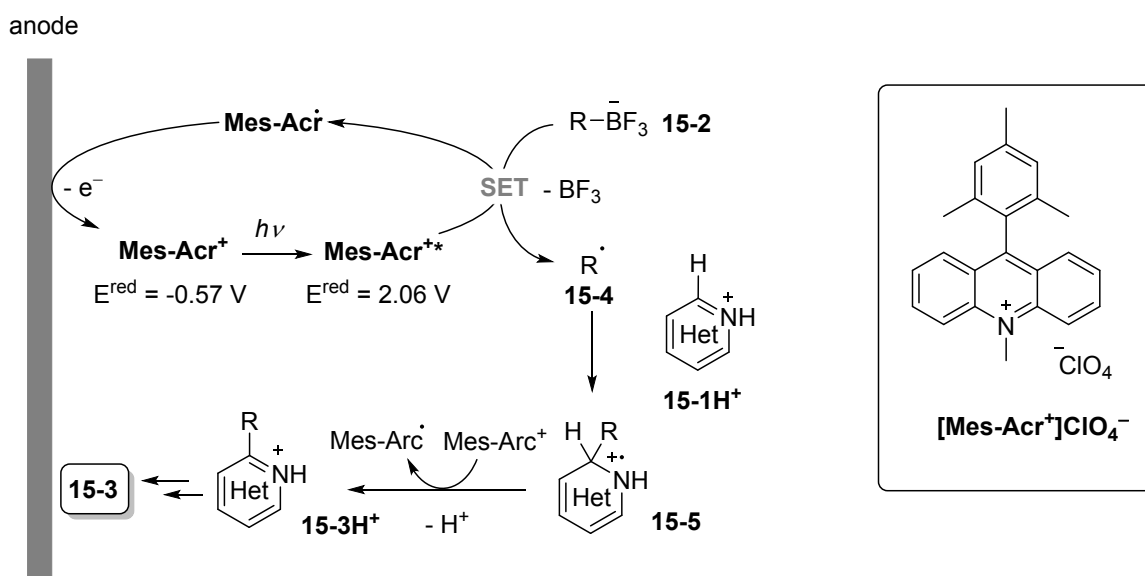
2.1.3. C–B deboronation of alkyl trifluoroborates and boronic acids

Organotrifluorobotates have recently become the preferred nucleophilic partners in cross-coupling reactions due to their ease of synthesis, high reactivity, relative stability under dry conditions, and excellent toleration of sensitive functional groups.[29] There has been increasing number of electrochemical radical coupling reactions using organotrifluoroborate salts as Csp^3-radical precursors in recent years.[30] In 2019, Yan et al reported an electrophotochemical method for Minisci-type alkylation of N-heteroarene with alkyl trifluoroborates.[31] The reactions proceeded smoothly with the organic dye [Mes-Acr]ClO$_4$ (9-mesityl-10-methylacridinium) perchlorate as the electrophotocatalyst and trifluoroacetic acid (TFA) as the additive, in the mixed solvent system MeCN/H$_2$O at room temperature (Figure 15a). Under blue LEDs irradiation, the highly oxidizing excited species [Mes-Acr$^+$]* ($E^{red} \approx 1.68$ V vs Fc/Fc$^+$) is formed. Single-electron transfer between [Mes-Acr$^+$]* and the alkyl trifluoroborate generates the alkyl radical **15-4**. No reaction occurred between the ground-state catalyst [Mes-Acr$^+$] ($E^{red} = -0.95$ V vs Fc/Fc$^+$) and the organotrifluoroborate substrate in the absence of light. The alkyl radical **15-4** then adds to the protonated substrate **15-5** to form the adduct **15-6**, which then undergoes thermodynamically favorable SET to the ground-state catalyst to furnish the product. The catalyst can be regenerated by anodic oxidation of the stable acridinium radical [Mes-Acr]•. Under these mild photocatalytic conditions, overoxidation of alkyl radicals usually does not occur and sensitive functional groups are well tolerated.

a. Reaction conditions

15-1 + **15-2** R−BF₃K

RVC | Pt
[Mes-Arc⁺]ClO₄⁻ (5 mol%)

TFA (1.0 equiv.)
MeCN/H₂O (2:1), Ar, rt, 10-28 h
CCE at 2.0 mA, undivided cell
blue LED

15-3

b. Proposed reaction mechanism

c. Representative examples

15-6, 65%   **15-7**, 78%   **15-8**, 72%   **15-9**, 65%
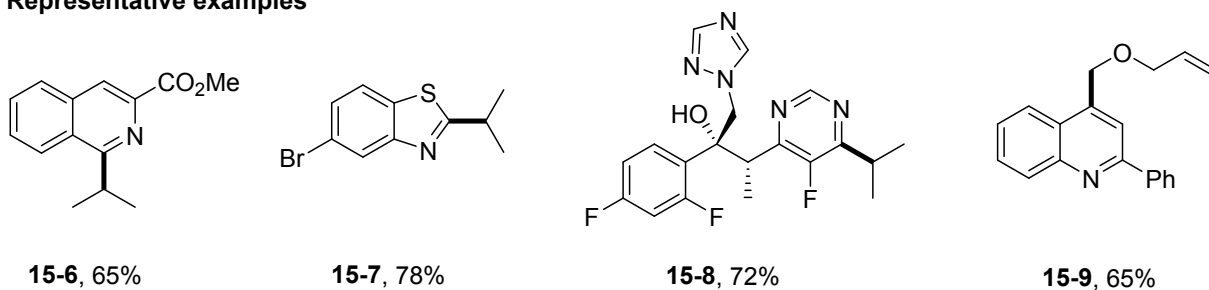
Figure 15. Electrophotochemical alkylation of *N*-heteroarenes by alkyl trifluoroborate salts. RVC = reticulated vitreous carbon. a. reaction conditions b. proposed reaction mechanism c. representative examples. [31]

Boronic acid derivatives, which are bench-stable and widely available, have also been demonstrated to be excellent precursors for carbon-radicals. The activation of boronic acids to form radical species often requires SET to stoichiometric oxidants such metal salts, persulfate, and hypervalent iodine.[30, 32, 33] In 2020, Yuan et al reported the use of a manganese salt as an electrocatalyst for the radical coupling reaction

between N-substituted benzimidazoles and alkylboronic acids (Figure 16).[34] CV experiments revealed that alkylboronic acids are first oxidized on the anodic surface to form the radical species **16-4**, as confirmed by electron paramagnetic resonance (EPR) experiments. The presence of Mn salt is crucial for the transformation, since only 4% yield of desired product was detected without Mn catalyst. $Mn(OAc)_3$ promotes the activation of boronic acid **16-2** through the persistent Mn^{III} species **16-5**, formed by direct SET with boronic acid substrate or by trapping of the radical **16-4** by a Mn^{II} species. Complex **16-5** then transfers the radical R• to the alkene moiety of the benzimidazole substrate **16-1** to regenerate the Mn^{II} and form the intermediate **16-6**. Subsequent radical cyclization and oxidation occur to deliver the benzo[4,5]imidazo[2,1-*a*]-isoquinolin-6(5*H*)-one product **16-3**. Protons are reduced on the cathodic side to form hydrogen gas as a byproduct.

a. Reaction conditions
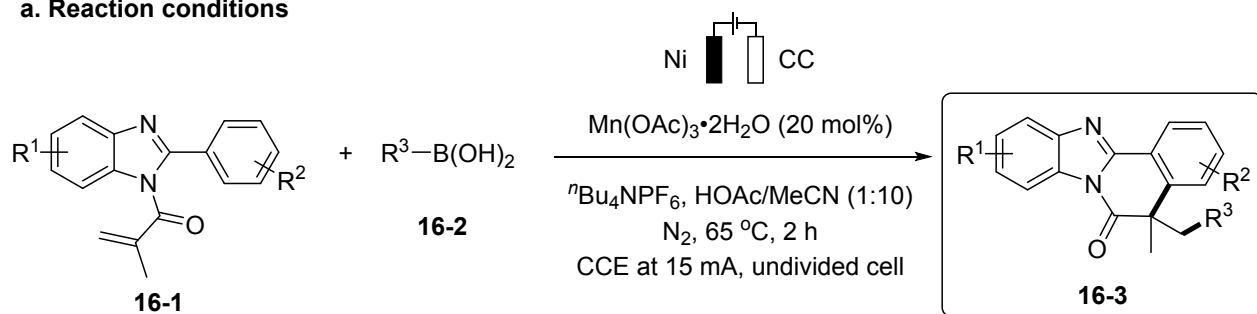
b. Proposed reaction mechanism

Figure 16. Mn-catalyzed electrochemical dual C–H bond activation for the synthesis of benzo[4,5]imidazo[2,1-a]isoquinolin-6(5H)-one derivatives. CC = carbon cloth; a. reaction conditions b. proposed reaction mechanism c. representative examples. [34]

2.2. Mediated reactions at cathodes
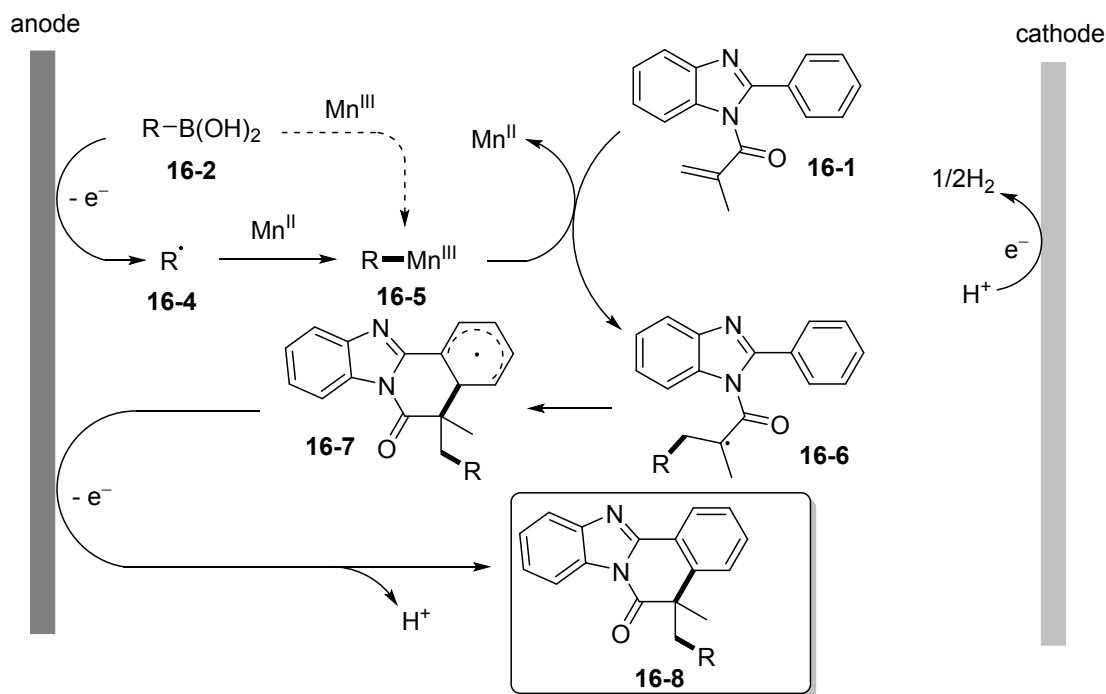
Compared to the anodic counterparts, the electroreductive methodologies for the generation of reactive carbon radicals remain relatively underexplored. This is due to a dearth of sufficiently reducing mediators and the need to use strong reducing conditions to activate certain functional groups. In contrast to the anodic processes, which are often coupled with proton reduction to form hydrogen gas as the sole by-product, the reductive electrolysis requires the use of "sacrificial" electron donors that can lead to undesirable side-reactions or electrode passivation.[8] In this section, we discuss the recent progress in electrocatalytic reductive coupling reactions that involve the generation of carbon-based radicals.

### 2.2.1. C-halogen bond cleavage

Nickel complexes are widely used as electrocatalysts in reductive chemistry.[8, 35, 36] Electrochemical methods allow for in situ generation of sensitive Ni species through cathodic reduction of shelf stable Ni precursors. Consequently, the reactive Ni species can undergo various reaction pathways involving oxidative addition to aryl halides or SET to alkyl halides that enables cross-electrophile coupling, C–H bond activation, alkene functionalization, and other C–heteroatom bonds formation.[37-39]

In 2020, Ackermann and co-workers developed a method for Csp^2—H alkylation of carboxylic acid derivatives with alkyl iodides (Figure 17).[40] 8-aminoquinoline was utilized as an efficient ortho-directing group under relatively mild conditions. Based on the mechanistic studies (Figure 17b), a nickel(II/III/I) redox manifold was proposed. The catalytic cycle starts with cathodic reduction to deliver Ni^I intermediate **17-4**, which then reacts with alkyl iodide to form the cyclometalated intermediate **17-5** after an irreversible C—H activation step. The Ni^{III} complex **17-5** is catalytically incompetent in the absence of electric current, which implies that cathodic reduction is essential for the generation of active Ni^{II} species **17-6**. Afterwards, single-electron transfer to alkyl iodide generates the intermediate **17-7**. Radical clock experiments suggest a homolytic cleavage of C—I bond in the alkylation step. Intermediate **17-7** then undergoes cathodic reduction to form the Ni^{III} complex **17-8**. Subsequently reductive elimination delivers the reaction product and the Ni^I species **17-4** is simultaneously regenerated upon coordination of substrate **17-1.** To compensate for the cathodic reduction, zinc was used as the sacrificial anode which also facilitates the alkyl iodide dissociation. A mechanism that involves zinc as potential redox mediator, or a transmetallation step from an alkylzinc iodide intermediate was ruled out based on control experiments.[40]

a. Reaction conditions

b. Proposed reaction mechanism

c. Representative examples

17-10, 77%   **17-11**, 72%   **17-12**, 50%
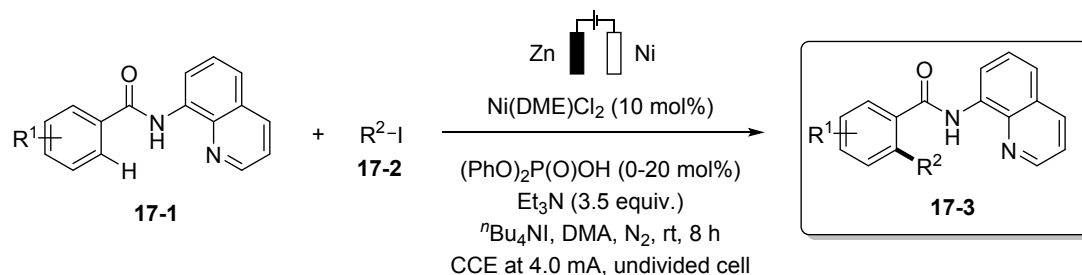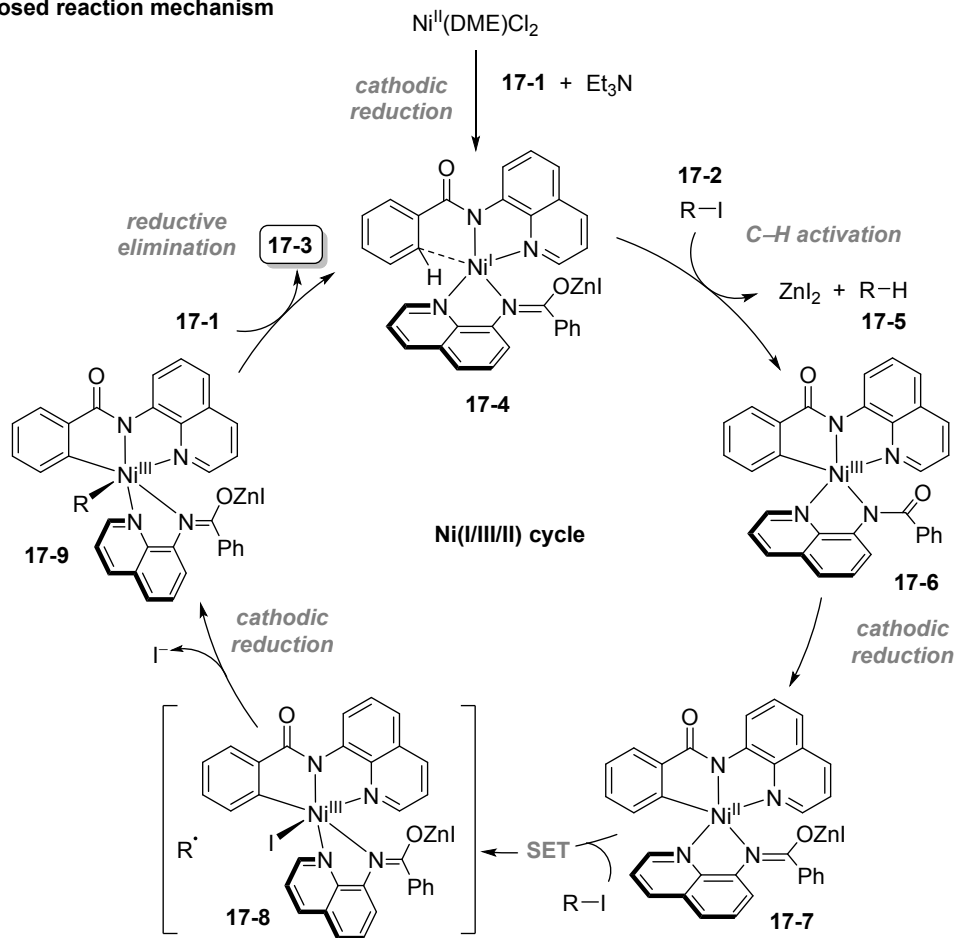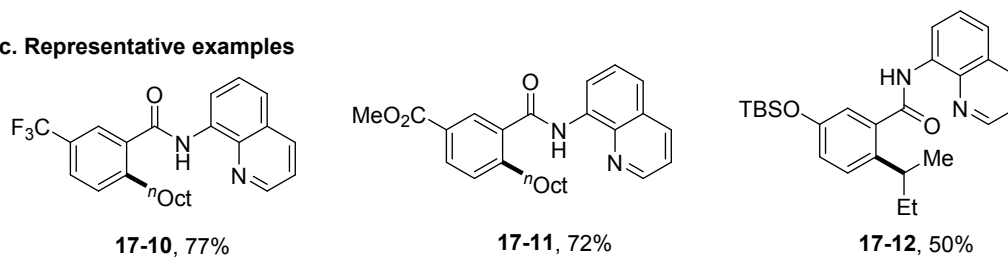
Figure 17. Electroreductive alkylation of Csp^2—H bonds by nickel Zn is a reducing agent; a. reaction conditions b. proposed reaction mechanism c. representative examples. [40]
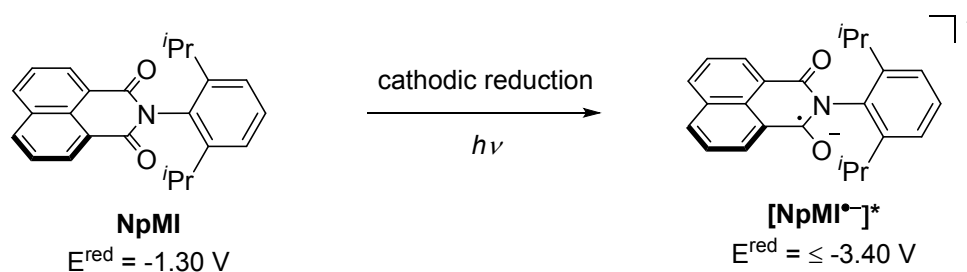
Aryl chlorides are among the most abundant, stable, and easily accessible carbon aryl radical precursors. The inherently low reactivity of the $C(sp^2)$–Cl bonds allows these types of bonds to be installed early in a synthetic process and further diversified in late-stage functionalization.[41, 42] The relatively inertness and high BDEs of the unactivated $C(sp^2)$–Cl bonds make their application in reductive cross-coupling a synthetic challenge.[43, 44] Due to their high reduction potentials (< -2.2 V vs Fc/Fc$^+$), which lie at or beyond the reduction limits of conventional visible-light photoredox catalysts, aryl chloride substrates are often overlooked in electroreductive and photoreductive chemistry.[35, 45, 46]

In 2020, Wickens and co-workers reported an electron-primed photoredox catalyst that can activate aryl chlorides for radical couplings (Figure 18).[47] The authors explored electrophotochemistry to overcome the energetic limitations of visible light by electrochemical reduction of an imide or diimide photocatalyst prior to excitation. NpMI (2-(2,6-diisopropylphenyl)- 1,8-naphthalimide) exhibited the best reactivity in reducing the challenging aryl chloride substrates. By addition of aryl radical-trapping agents like N-methylpyrrole or triethyl phosphite, the coupling products can be formed selectively under mild controlled current electrolysis conditions. Notably, an exceptionally electron-rich aryl chloride substrate (-3.80 V vs Fc/Fc$^+$) can be converted to the C–C or C–P coupling product in 47% and 51% yields, respectively. Other aryl chlorides bearing strong electron-donating groups, and potentially sensitive reducible functional groups are also compatible with the reaction conditions (Figure 18c).

a. Reaction conditions
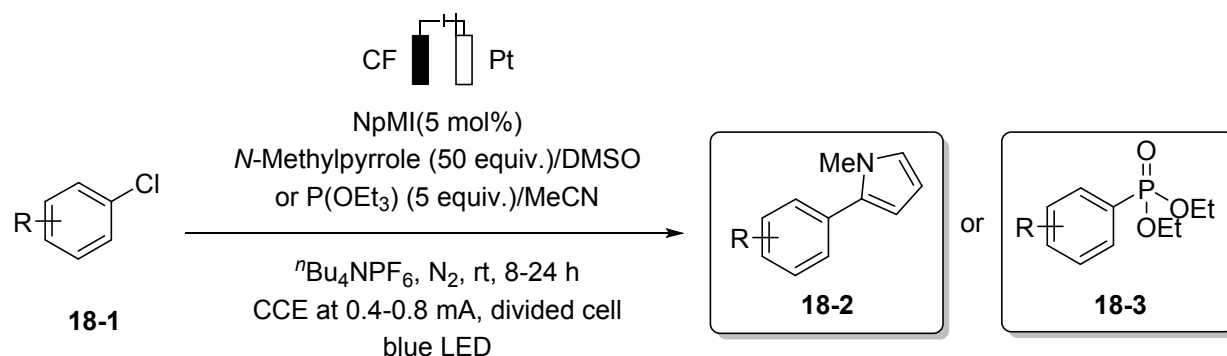
b. Accessing highly reducing species with electrophotochemistry

c. Representative examples

18-4, 53%   **18-5**, 41%   **18-6**, 47%   **18-7**, 81%

18-8, 89%   **18-9**, 51%   **18-10**, 65%   **18-11**, 82%
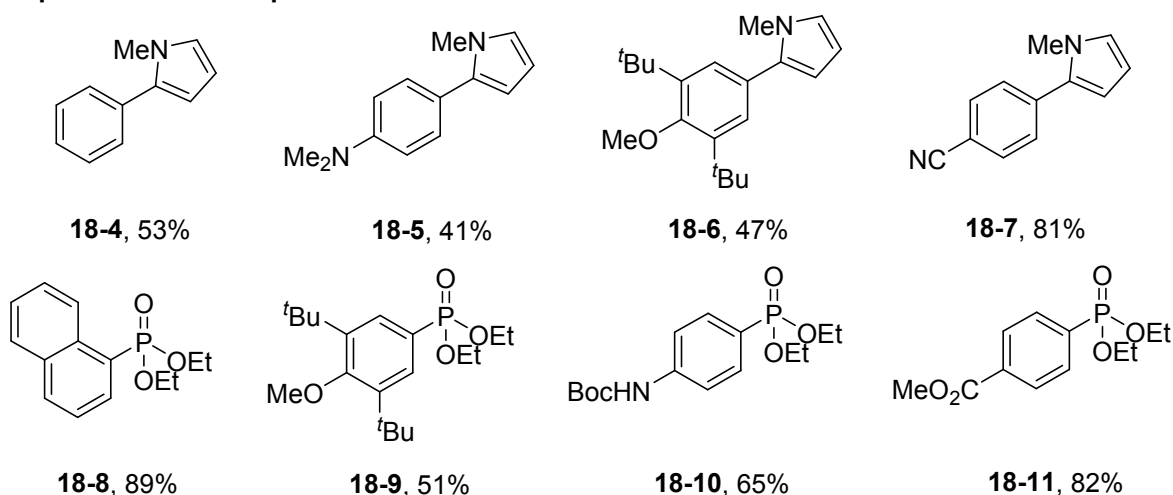
Figure 18. Reaching extreme electroreductive conditions by electrophotocatalysis. CF = carbon felt; a. reaction conditions b. proposed reaction mechanism c. representative examples. [47]

2.2.2. C–C bond cleavage

In 2018, Li et al demonstrated a complementary approach to electrochemical Ni-catalyzed cross coupling of N-hydroxyphthalimide (NHP) esters and (hetero)aryl halides.[48] The reaction proceeds under mild conditions in a divided electrochemical cell and employs triethylamine as the sacrificial reductant on the anodic side (Figure 19). The catalytic cycle is initiated by cathodic reduction to deliver the active Ni^0 species. Subsequent oxidative addition of aryl halide forms the Ni^{II} complex. At the same time, single-electron transfer from the electrode surface to the NHP ester, followed by decarboxylation produces the

radical species **19-9**. This reductive decarboxylation pathway is also supported by radical clock experiments. Upon coordination of **19-9** and SET to the preformed Ni^{II} complex **19-6**, reductive elimination occurs to deliver the coupling product and regenerates the Ni^{I} species back to the catalytic cycle. The major reduction event is the reduction of the Ni^{II} precursor at -1.19 V vs Fc/Fc^+, as supported by CV experiments. This reduction potential is less negative than the reductive potential of both NHP ester at around -1.59 V vs Fc/Fc^+ and iodobenzene at -2.69 V vs Fc/Fc^+.

In 2019, Koyanagi et al also developed an analogous strategy for the Csp^2-Csp^3 electrochemical cross-coupling between aryl iodides and NHP esters, which are generated *in situ* upon reaction of carboxylate salts with PITU reagent (PITU = *N*-hydroxyphthalimide tetramethyluronium hexafluorophosphate).[49] The reaction can be performed in an undivided electrolysis cell with zinc as the sacrificial anode, which simplifies overall complexity compared to the common divided cell setup.

Additionally, Lian et al reported a similar Ni-mediated system with the coupling partner extended to quinoxalinone Csp^2—H bonds.[50] The authors proposed that SET from the Ni^{II}/Ni^{I} redox couple would facilitate the reduction of NHP esters to form the corresponding radical species upon CO_2 loss, though direct electron transfer pathways from the cathode to the NHP ester are also possible. Upon Minisci-type radical trapping by quinoxalinone, the formed radical cation is further oxidized to generate the desired coupling product with the assistance of Ni coordination.

a. Reaction conditions
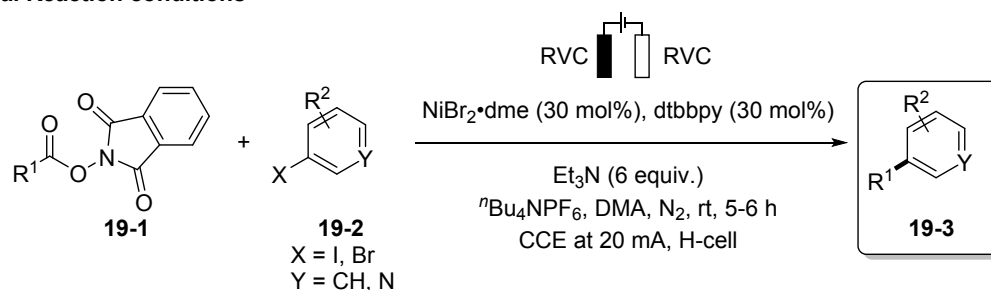
b. Proposed reaction mechanism
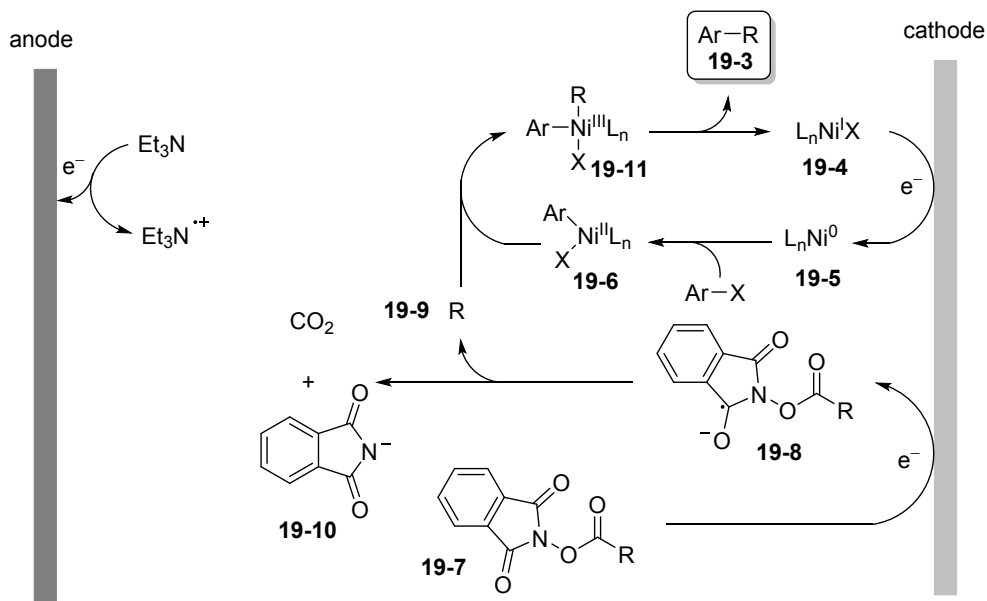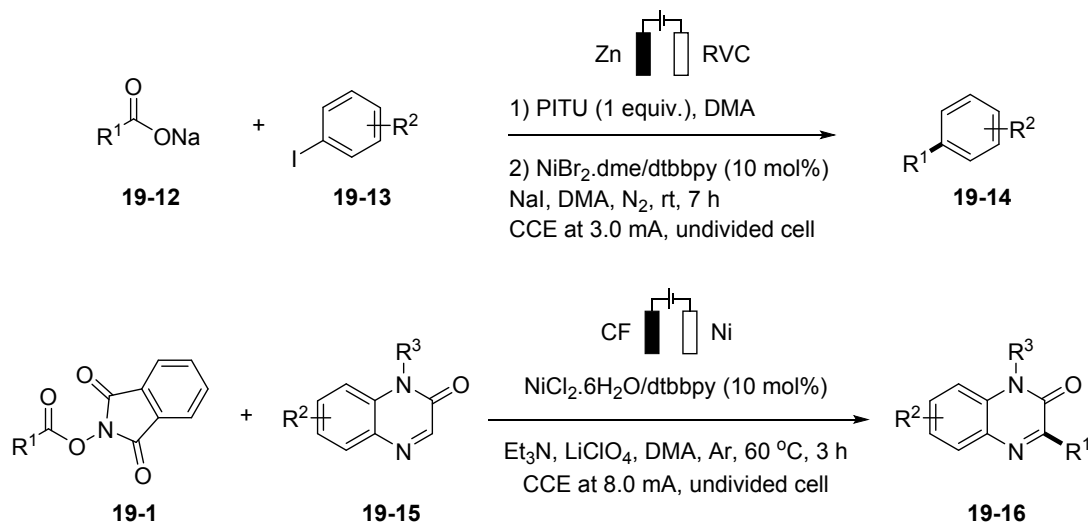

c. Recent advances

Figure 19. Ni-mediated reductive functionalization of arenes and NHPI-esters; a. reaction conditions b. proposed reaction mechanism c. recent advances. [48]

In 2020, Zhang et al reported an electrochemical Ni-promoted decyanative pyridylation of electron-poor alkenes, using 4-cyanopyridine as the precursor to the pyridine moiety.[51] A variety of coupling products are obtained in moderate to good yield under optimal reaction conditions (Figure 20). Based on CV experiments, the authors proposed that metal additive $Ni(acac)_2$ diminished the reduction of 4-cyanopyridine by coordination and promoted the reduction of the Michael-acceptor substrate to form the corresponding radical anion. Following that, a radical-radical cross-coupling with an electrogenerated cyanopyridyl radical anion or a radical addition to a Ni-coordinated cyanopyridine yields the C–C coupling product after elimination of cyanide anion.

a. Reaction conditions

b. Representative examples

20-4, 51%   **20-5**, 22%   **20-6**, 54%   **20-7**, 55%
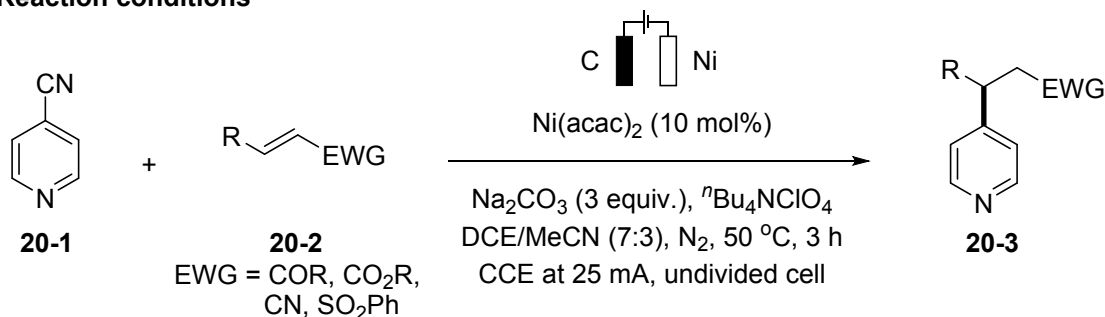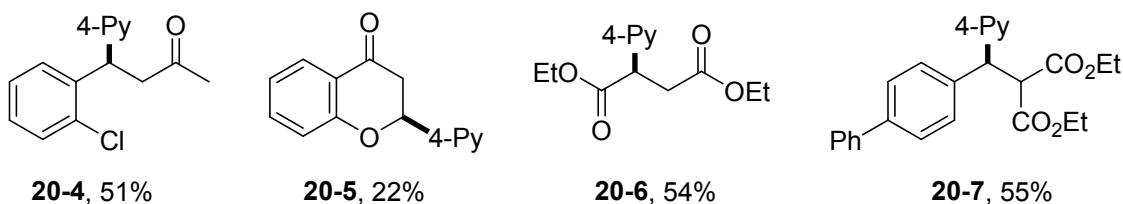
Figure 20. Ni-mediated electroreductive pyridylation of electron-deficient alkenes; a. reaction conditions b. proposed reaction mechanism c. representative examples. [51]
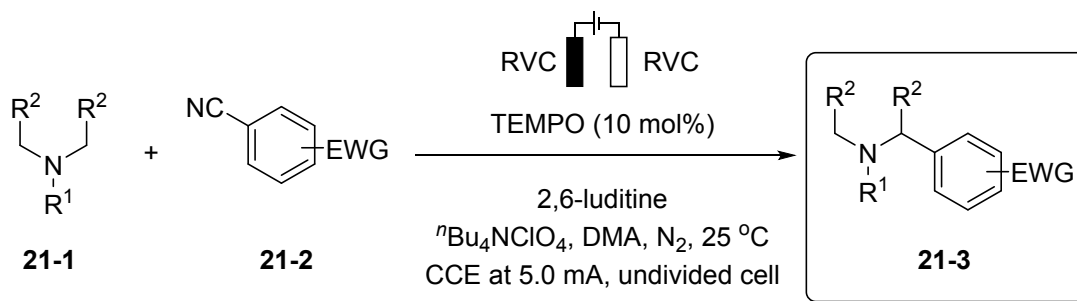
2.3. Paired electrolysis

Paired electrolysis has recently attracted significant interest for its ability to perform two desirable electrochemical half reactions simultaneously within the reaction system. This effective and atom-economical synthetic strategy has found applications in industrial electrosynthesis and energy conversion processes.[36, 52, 53] The big challenge in paired electrolysis arises from the competition between interelectrode mass transfer of reactive radical intermediates, generated from both anodic and cathodic events, and their undesirable degradation pathways. Considering these challenges, the reaction design for paired electrolysis requires carefully controlled reaction conditions and selection of the coupling partners to enhance the reaction selectivity. In some examples described in previous sections the paired reactions on the counter electrode are crucial for overall transformation and in these instances, the whole system can be considered paired electrolysis. In this section, we describe recent advances in which paired electrocatalysis is ingeniously implemented to enhance the reaction efficiency and selectivity.

In 2019, Ma et al reported a method for $C(sp^3)$–$C(sp^2)$ radical coupling between alkylamines and electron-deficient benzonitriles (Figure 21).[54] This cross coupling reaction of tertiary amine and benzonitrile could be accomplished through convergent paired electrolysis, in which the anodically generated α-amino radical reacts with the arene radical anion formed at the cathode, yielding the final coupling product.

TEMPO(2,2,6,6-Tetramethylpiperidine-1-oxyl)/TEMPO$^+$ redox couple, which has previously been utilized in various electrooxidation chemistries,[55] is used to promote the oxidation of amine **21-4** on the anodic side to form the radical cation species **21-5**. 2,6-lutidine is an added base that facilitates the deprotonation of amino radical cation **21-5**, while shifting the equilibrium to TEMPO. Additionally, it greatly increases the catalytic current as observed in CV experiments.[54] The carbon-radical species **21-6** then couples with the radical anion **21-8**, formed upon cathodic reduction of the benzonitrile substrate, to form the key intermediate **21-9**. Subsequent elimination of cyanide and rearomatization of **21-9** affords the desired product **21-10**. Interestingly, the oxidation potentials of amine substrates inversely associate with the rates of oxidation and are important to drive this paired electrolysis, since no coupling products are detected in the case of electron-deficient amines.

a. Reaction conditions

b. Proposed reaction mechanism

c. Representative examples

21-11, 79%   **21-12**, 46%   **21-13**, 41%   **21-14**, 44%
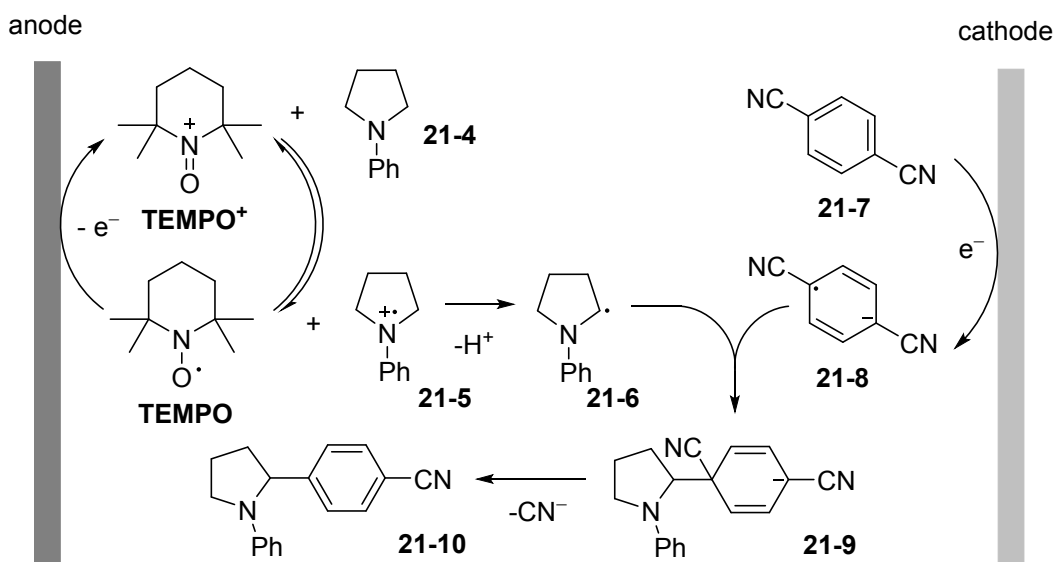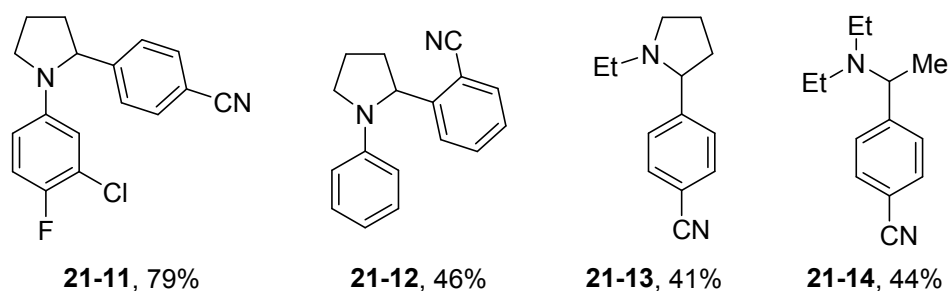
Figure 21. Electrochemical arylation of α-amino C(sp^3)-H bonds by convergent paired electrolysis; a. reaction conditions b. proposed reaction mechanism c. representative examples.[54]

Moving to mediated cathodic reduction, the same research group developed an electrochemical nickel-catalyzed aminomethylation of aryl bromides (Figure 22).[37] The combination of Ni and dtbbpy (4,4′-Di-tert-butyl-2,2′-dipyridyl) ligand activates the aryl bromide substrate through a conventional oxidative addition pathway to form complex **22-5**, initiated by cathodic reduction of Ni^{II} to the active Ni^{I} complex **22-4**. This intermediate then undergoes a second cathodic reduction to form the Ni^{II} species **22-6**.

Meanwhile, α-amino carbon radical **22-8** is simultaneously formed upon oxidation and deprotonation at the anode. This radical intermediate is then rapidly captured by the Ni^{II} complex **22-6**, generating the high-valent Ni^{III} intermediate **22-9**. [37, 56] Subsequent reductive elimination occurs to produce the coupling product **22-3** and regenerate the Ni^I complex. Under these mild electrolysis conditions, a broad range of substrates bearing sensitive functional groups are well-tolerated with excellent selectivity.

a. Reaction conditions

b. Proposed reaction mechanism

c. Representative examples

22-10, 76%   **22-11**, 71%   **22-12**, 58%
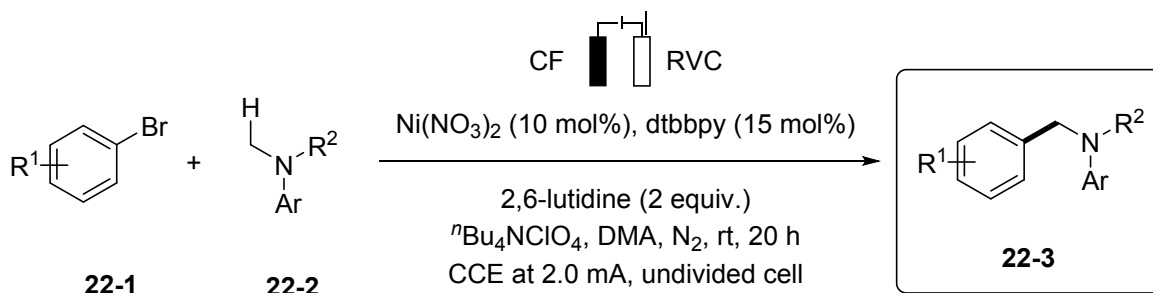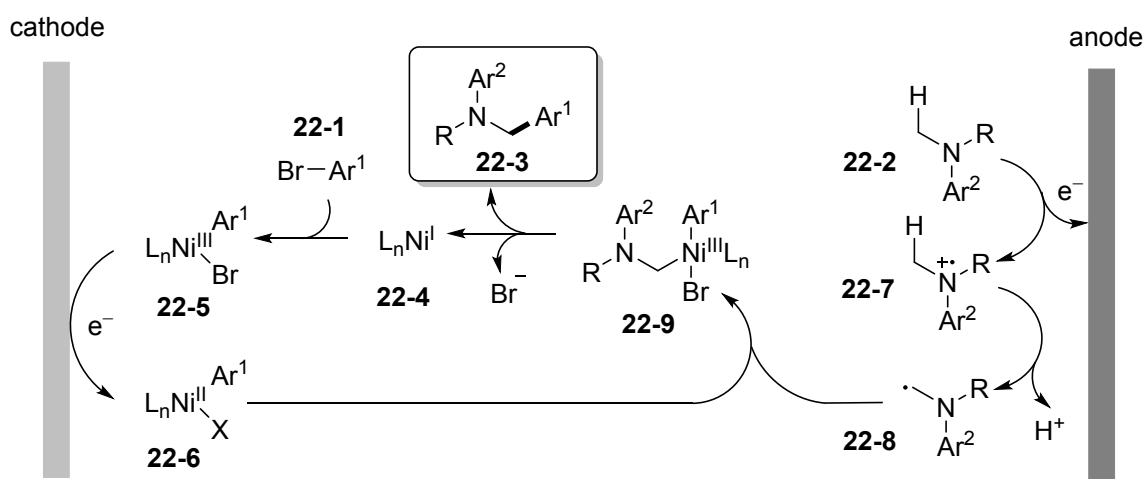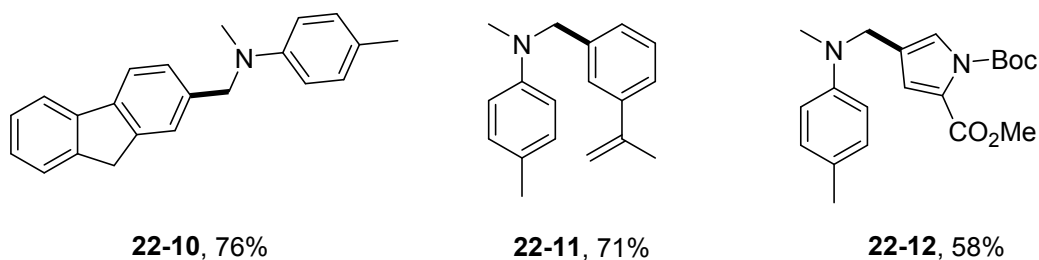
Figure 22. Paired electrolysis for redox-neutral cross-coupling between methylanilines and aryl bromide via Ni catalysis. a. reaction conditions b. proposed reaction mechanism c. representative examples.[37]

In 2021, Luo et al described the use of convergent paired electrolysis to achieve a similar radical coupling reaction between aryl or alkenyl bromides with organofluoroborate salts via nickel catalysis (Figure 23).[38] The coupling partners were selected through extensive CV screening between potential substrates and nickel complexes. The combination of anodic oxidation of benzyl trifluoroborate salts and cathodic

reduction of organonickel intermediates, formed upon oxidative addition of the aryl bromide substrates, affords the desired coupling products in high to excellent yields. Mechanistic studies suggest that electricity is crucial for the transformation despite the redox-neutral nature of the designed paired electrolysis scenario. The reaction is initiated by electroreduction of Ni^{II} precursor **23-6** to Ni^{I} complex **23-7**, followed by oxidative addition of aryl bromide or alkenyl bromide substrate to form Ni^{III} intermediate **23-8**. This Ni^{III} intermediate then undergoes a second reduction at the cathode to form the Ni^{II} complex **23-9**. The addition of anodically generated alkyl radical **23-10** to the Ni^{II} complex **23-9**, followed by a final reductive elimination furnishes the desired coupling product and turn over the Ni^{I} catalyst **23-7**. Under this relatively mild set of reaction conditions, a wide variety of benzyl trifluoroborates and bromides are successfully coupled, inclusive of ones bearing sensitive functional groups such as acetals, aldehyde, and protected amines.

a. Reaction conditions

b. Proposed reaction mechanism

c. Representative examples

23-12, 86% (from ArCl) 93% (from ArBr)

23-13, 78% (from ArBr)

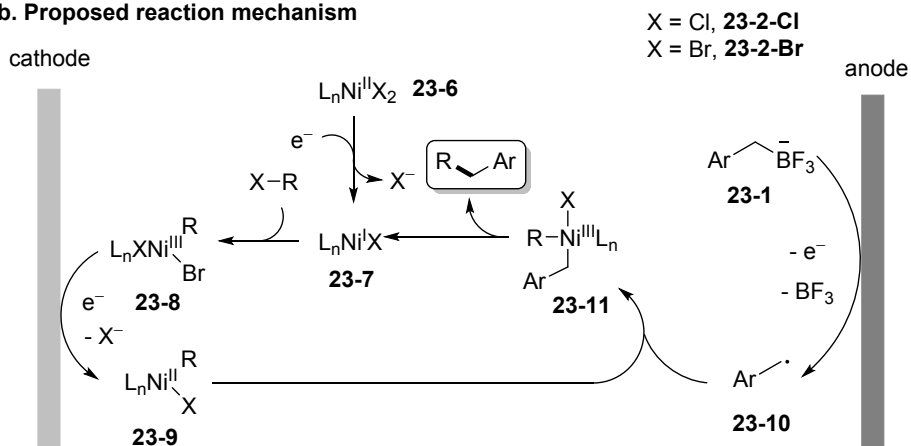**23-14**, 81% (from ArBr)

23-15, 86%
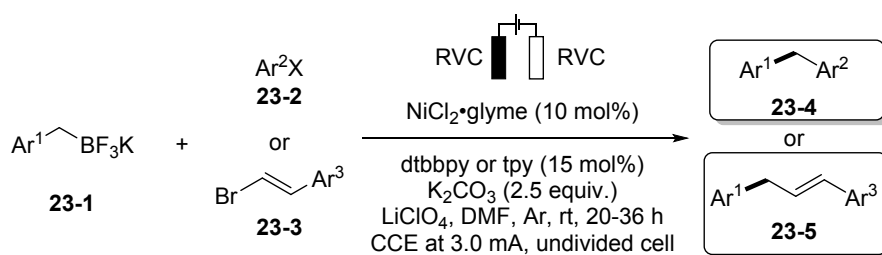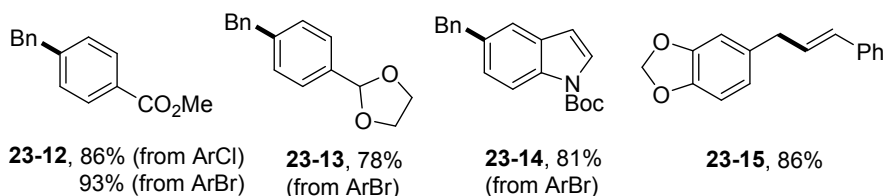
Figure 23. Paired electrolysis for redox-neutral cross-coupling between organic bromides and organotrifluoroborate salts via Ni catalysis; a. reaction conditions b. proposed reaction mechanism c. representative examples. [38]

3. C–N Bond Coupling Reactions

Historically, C-N bond coupling chemistry has been heavily dependent on the use of stoichiometric amounts of chemical oxidants, which can be expensive and generate large amounts of waste.[57] These reactions are especially critical for synthesis within the biomedical industry and it is important that cheaper, cleaner chemistry is developed for this process.[58] This section highlights recent advancements in electrochemical and electrophotocatalytic C–N coupling reactions. While C–C bond formation was enabled at both cathodes and anodes, the mediated C–N bond-forming chemistries are limited to exclusively anodic processes.

3.1 Decarboxylative C–C bond cleavage

In 2018, Lin and Huang demonstrated the successful N-formylation of amines through electrochemical decarboxylation of glyoxylic acid.[59] The optimized reaction conditions (Figure 24) involve reacting N-methylaniline with glyoxylic acid along with 10 mol % $Cu(OAc)_2 \cdot 2H_2O$ and 20 mol % $NiCl_2 \cdot 6H_2O$ in the presence of cesium carbonate, sodium perchlorate electrolyte, and DMSO (dimethylsulfoxide) solvent in an undivided cell with a 5 mA constant current for 10 hours. Yield decreased when the $Cu(OAc)_2 \cdot 2H_2O$ and Ni salt were omitted or the current was increased or decreased. Additionally, only trace product was obtained without the presence of cesium carbonate and no product was obtained without an electric current present.

The proposed mechanism for this reaction is illustrated in Figure 24b. Cesium carbonate deprotonates the acid, which is then condensed with aniline to from the **24-4** intermediate. This species then loses a proton to yield **24-5**, which exists in equilibrium with **24-6**. The **24-6** intermediate is then oxidized by the cupric acetate and decarboxylation occurs to produce **24-7**. This species loses one electron and one proton to form **24-3**, the desired formylation product, as a result of electron-donating substituent at the alpha position. In the presence of substoichiometric amounts of radical scavengers, the reaction yields decreased.

Both primary and secondary amines are good substrates, as well as both aliphatic and aromatic amines. Some applicable examples are shown in Figure 24c. Amines with bulky substituents were not tolerated.

a. Reaction conditions

b. Proposed reaction mechanism

c. Representative examples

24-8, 93%   **24-8**, 76%   **24-8**, 78%   **24-8**, 36%   **24-8**, 87%
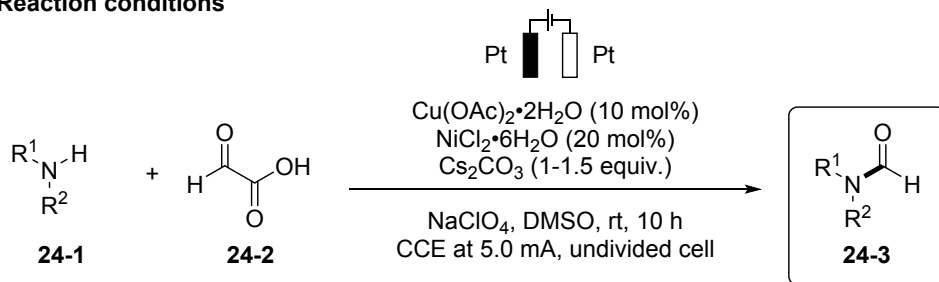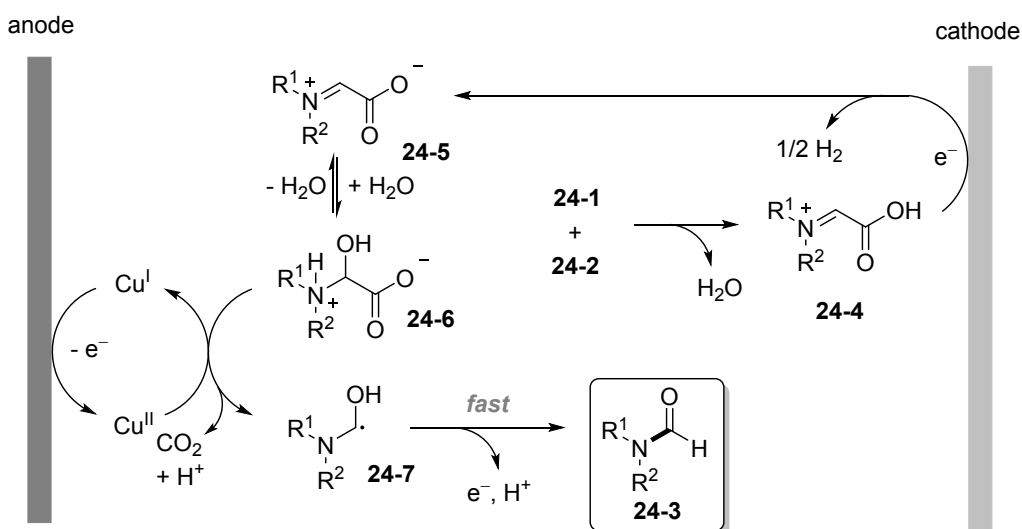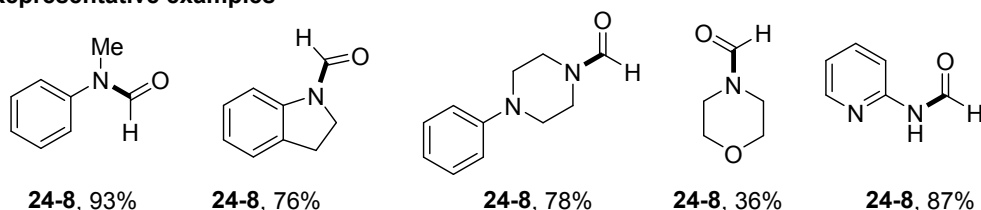
Figure 24. Electrochemical *N*-formylation of amines via copper-catalyzed decarboxylation of glyoxylic acid. a. reaction conditions b. proposed reaction mechanism c. representative examples.[59]

3.2 C–H bond activation

In 2020, Niu et al published their methodology for the use of nucleophilic NaN_3 as an azide source to perform oxidative azidation of $C(sp^3)$-H bonds using a manganese electrophotocatalytic method to form various alkyl azides.[57] The optimized reaction is shown in Figure 25 and involves the reaction of $C(sp^3)$-H bonds with NaN_3 in the presence of a Mn catalyst, a photocatalyst, ligand, acid, and electrolyte under blue LEDs and 4.5 mA of current over 15 hours. Ligand choice was demonstrated to be important, as ligands with electron withdrawing groups or steric hindrance impaired yield, and electron rich ligands led to no product at all.

The proposed mechanism for this reaction is illustrated in Figure 25b and suggests that NaN_3 is directly oxidized to the azide radical on the anodic surface while $L_nMn(II)$ **25-4** simultaneously undergoes anodic oxidation to form the $L_nMn(III)-N_3$ intermediate **25-5**. Kinetic studies indicated that cleavage of $C(sp^3)$-H is the rate determining step and that concentration of azide radical and **25-5** determined the capture of the radical to produce the final product. Irradiation of the photocatalyst **26-6** then results in the hydrogen atom transfer (HAT) event to generate the $C(sp^3)$ radical **26-10**, which is followed by final alkyl azide product formation from azide transfer from **25-5** to an alkyl radical, while simultaneous Mn(II) turnover occurs. Other mechanistic possibilities include HAT regeneration via anodic oxidations, the possibility that **25-5** is involved in turnover of the photocatalyst, and that the azide radical could also potentially abstract the hydrogen from the $C(sp^3)$-H bonds to generate the $C(sp^3)$ radical. The proposed mechanism is supported by radical inhibition and CV expe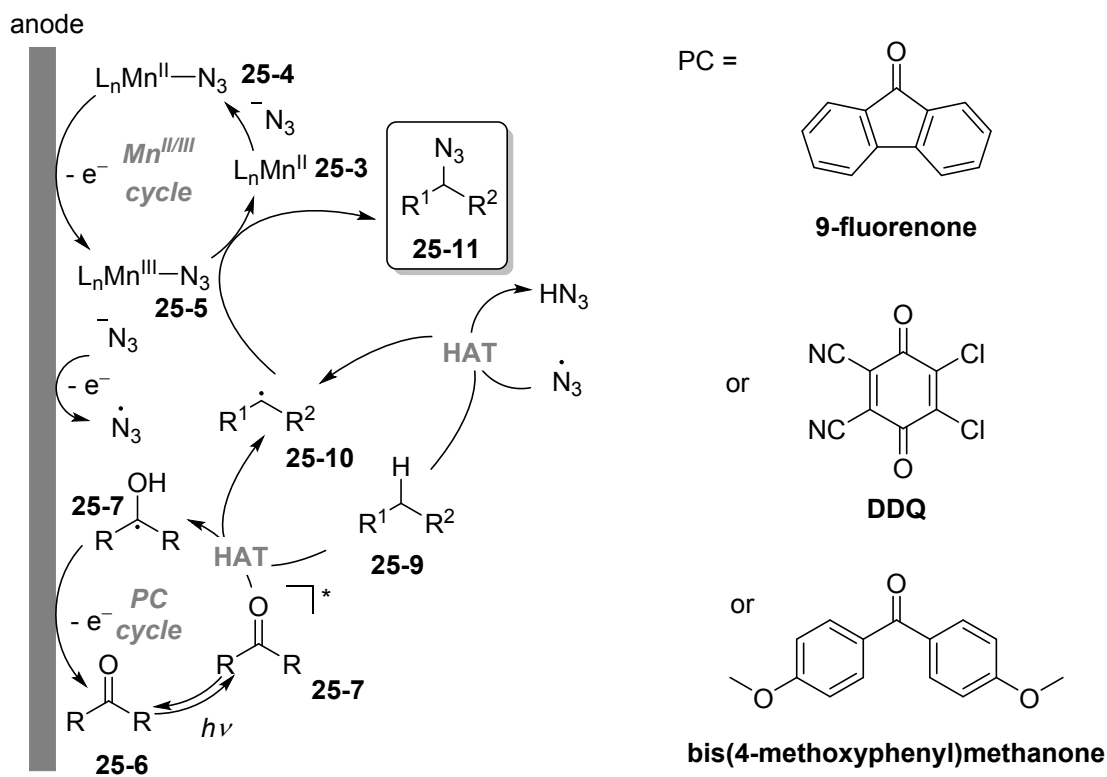riments. 5,5-Dimethyl-1-pyrroline N-oxide (DMPO) captured the azide radical, demonstrating its existence during the reaction. Carbon radicals were also confirmed during irradiation of HAT photocatalyst, suggesting that generation of $C(sp^3)$ radical most likely comes from the photocatalytic process and abstraction of the N_3 radical. Cyclic voltammetry experiments showed that oxidation of NaN_3 to the azide radical on the anodic surface was facile and that conversion of **25-3** to **25-5** would be unrealistic with direct oxidation only.

It was noted that the azidation reactivities of tertiary $C(sp^3)$-H bonds were generally better than secondary, possibly due to a more stable radical. Tertiary aliphatic $C(sp^3)$-H bonds specifically demonstrated selectivity in substrates that could be important for implementing nitrogen functionality at the tertiary alkyl group.

a. Reaction conditions

CC █ ▢ Pt

PC (5.5-11 mol%)
MnF$_2$ (10 mol%), 1,10-Phen (20 mol%)

$C(sp^3)\!-\!H$ + NaN$_3$ $\xrightarrow{\hspace{3cm}}$ $C(sp^3)\!=\!N_3$

25-1

KBr (0-40 mol%), LiClO$_4$, TFA
MeCN/DCE/HOAc, N$_2$, 35 °C, 15-24 h
CCE at 4.5 mA, undivided cell
blue LEDs

25-2

b. Proposed reaction mechanism

anode

L$_n$Mn^{II}—N$_3$ **25-4**

$^-$N$_3$

- e$^-$ ***Mn$^{II/III}$ cycle***

L$_n$Mn^{II} **25-3**

N$_3$
R^1 R^2
25-11

L$_n$Mn^{III}—N$_3$
25-5

$^-$N$_3$

- e$^-$

·N$_3$

HN$_3$

HAT

·N$_3$

R^1 · R^2
25-10

OH
25-7
R R

HAT

H
R^1 R^2
25-9

PC cycle

- e$^-$

O
R R
*

O
R R
25-7

O
R R
hv
25-6

PC =

9-fluorenone

NC ⟶ O ⟶ Cl
NC ⟶ O ⟶ Cl
DDQ

or

or

bis(4-methoxyphenyl)methanone

c. Representative examples

Ph
N$_3$
Ph
25-12, 99%

N$_3$
25-13, 69%

N$_3$
O
25-14, 39%

Cl
N$_3$
25-15, 54%

MeO
N$_3$
Br
25-16, 43%
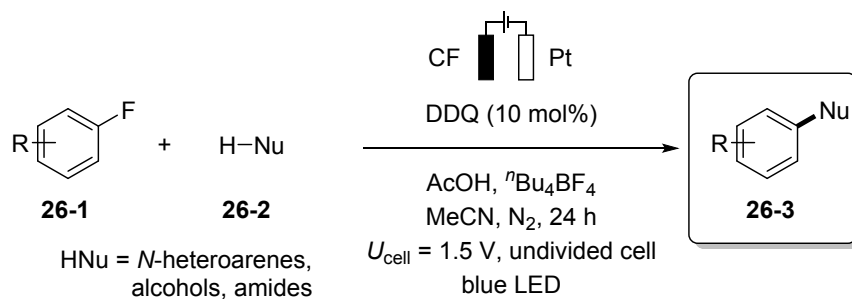
Figure 25. Manganese-mediated oxidative Csp^3–H azidation under electrophotocatalytic conditions. a. reaction conditions b. proposed reaction mechanism c. representative examples. [57]

In a related study, Huang and Lambert performed electrophotocatalytic nucleophilic aromatic substitution (S_NAr) reactions on unactivated aryl fluorides using mild conditions and without strong base, which is significant because high temperatures and strong bases have historically been necessary to transform inactivated substrates.[60] The optimized reaction conditions are shown in Figure 26. This reaction was first discovered using the trisaminocyclopropenium (TAC$^+$) electrocatalyst, which will be discussed in more detail later in this section, but 2,3-dichloro-5,6-dicyanoquinone (DDQ) was found to provide a better yield.
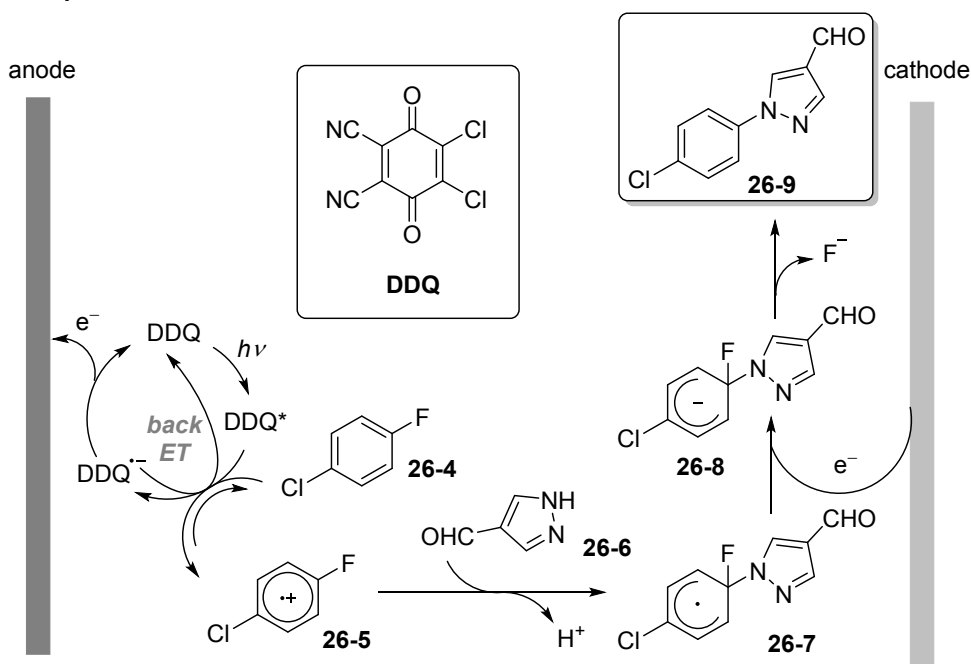
A proposed mechanistic rationale for this reaction is shown in Figure 26b. A potently oxidizing excited state species DDQ* is produced by the photoexcitation of DDQ, which is strong enough at E_{red} = 2.80 V vs Fc/Fc$^+$ (originally measured as 3.18 V vs SCE) to go on to oxidize the fluoroarene **26-4**. The pyrazole **26-6** then performs a nucleophilic attack, which produces the radical **26-7**. It is proposed that **26-7** then undergoes a single electron reduction in order to expel the fluoride leaving group to produce the final desired product, **26-9**. These reaction conditions also demonstrated the possibility for chemoselectivity, notably producing only product **26-10** when pyrazole and a 1-1 mixture of 1-chloro-4-fluorobenzene and 1-fluoro-2,4-dinitrobenzene were subjected to standard reaction conditions, with the aryl fluoride left intact. This was also observed with the selective conversion of 1-chloro-4-fluorobenzene to **26-10** in the presence of 4-fluoroanisole, which did not react.

In a follow-up study DDQ was used to perform electrophotocatalytic heterofunctionalization of arenes, including oxidant-free hydroxylation, alkoxylation, and amination reactions.[61] While the reaction was initially performed under conditions mimicking their 2020 study, conditions were optimized to use 6 equivalents of LiClO$_4$ as the electrolyte, 50 equivalents of water, blue LEDs, and U_{cell} = 1.5 V in an undivided cell for 24 hours (Figure 27a). The mechanism of this reaction is speculated to be very similar to Figure 26b, with the primary difference being that DDQ would be regenerated by anodic oxidation by produced DDQH$_2$ with reduction of protons to hydrogen gas at the cathode to complete the electrochemical cycle. The scope of this reaction is broad; under the proposed conditions, water, alcohols, acids, amides, or carbonates can be appended to arenes without the need for external chemical oxidants. Examples of products are provided in Figure 27c. Notably, alkoxybenzenes and phenols did not undergo reaction, likely due to the outcompetition of the nucleophilic attack to the transient radical cation intermediate by a rapid back-electron transfer process. Amines were also not reactive, most likely due to acidic conditions. Additionally, an optimized continuous flow system was developed to reduce reaction time. By coupling three photochemical channels to an undivided electrochemical cell and using a residence time of 3 minutes and a controlled potential of 1.5 V, a 4 mmol scale reaction produced a 60% yield of phenol in 22 hours.

a. Reaction conditions

HNu = *N*-heteroarenes, alcohols, amides

b. Proposed reaction mechanism

c. Representative examples

26-10, 73%   **26-11**, 53%   **26-12**, 43%   **26-13**, 56%
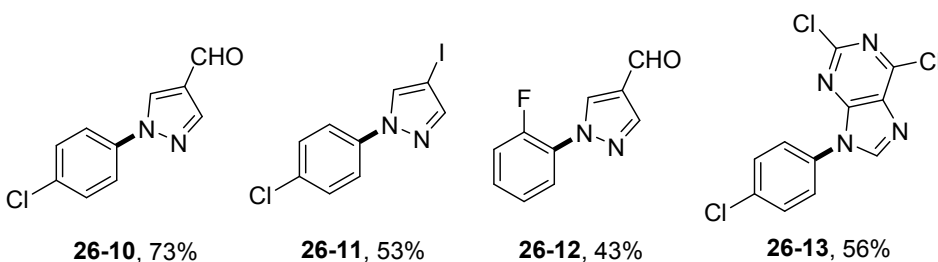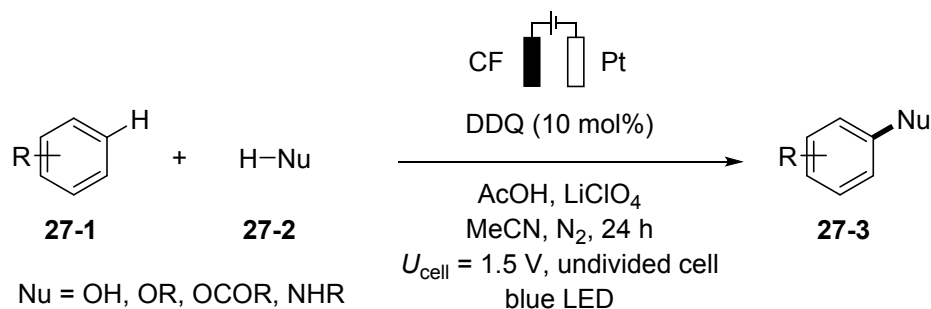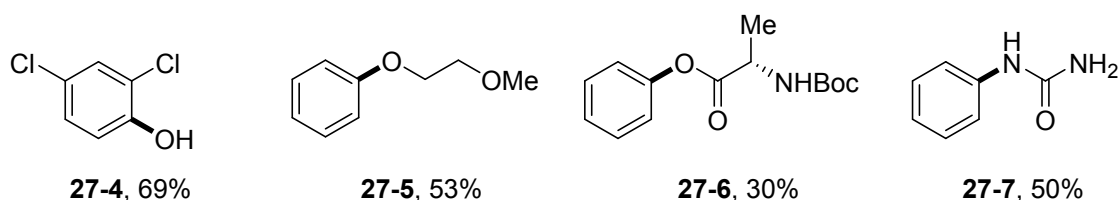
Figure 26. DDQ-mediated activation of aryl fluorides under electrophotocatalytic conditions; a. reaction conditions b. proposed reaction mechanism c. representative examples. [60]

a. Reaction conditions

Nu = OH, OR, OCOR, NHR

b. Representative examples

**27-4**, 69%　　　　**27-5**, 53%　　　　**27-6**, 30%　　　　**27-7**, 50%

Figure 27. DDQ-mediated oxidative functionalization of unactivated Csp^2–H bond under electrophotocatalytic conditions; a. reaction conditions b. representative examples. [61]
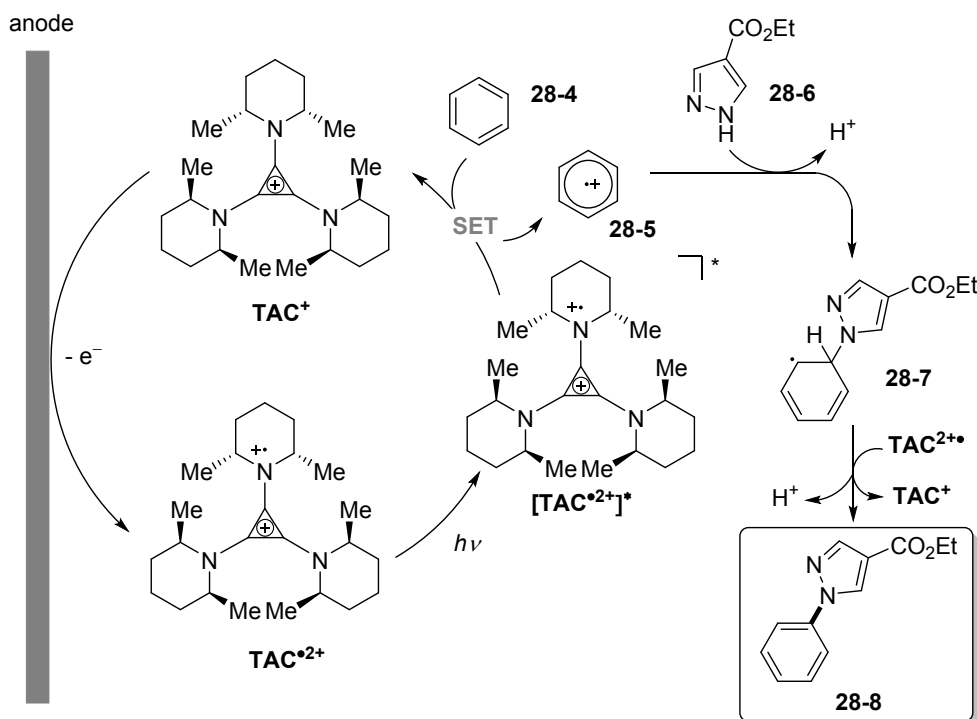
In a different example, Huang et al showed that TAC$^+$ could be used as a potent yet selective oxidative electrophotocatalyst.[62] TAC$^+$ meets the challenging criteria that the electrocatalytic species must be able to yield a stable intermediate via a one-electron transfer event, absorb visible light once oxidized, remain in the excited state long enough to interact with the substrate, and is stable throughout the reaction process. The TAC$^+$ is unique in that it can be reversibly oxidized to the corresponding radical dication, which when photoexcited has a calculated excited state reduction potential of $E^*_{1/2}$ = 2.95 V vs Fc$^+$/Fc (originally reported as 3.33 V vs SCE). Under the optimized reaction conditions shown in Figure 28a, it was shown that TAC$^+$ catalyzes the reaction between benzene and pyrazole to produce **28-6** (Figure 28b) cleanly with 65% yield. It was observed that the ^{1}H NMR spectrum of the electrophotocatalytic product was much cleaner than the spectrum resulting from a purely direct electrolysis procedure.

The proposed mechanism for TAC$^+$ electrophotocatalysis is illustrated in Figure 28b. The radical dication is generated by electrochemical oxidation of the TAC$^+$, which is followed by photoexcitation to produce the reactive intermediate. The intermediate can go on to oxidize benzene via single-electron transfer to produce the radical cation **28-5**, which allows the reaction to proceed to nucleophilic trapping by **28-6**, deprotonation to yield the radical **28-7**, further oxidation of **28-7**, and ultimately re-aromatization that produces the product **28-8**. The authors clarify that although this is the most likely mechanistic explanation, further study is warranted. As far as the scope of the reaction, carboxyl, aldehyde, and ketone functional groups were all well-tolerated. It was shown that the regioselectivity of azole coupling was significantly influenced by the chosen azole partner. Although TAC$^+$ demonstrated very strong oxidizing power, the limit was discovered to be the trifluoromethyl group, which proved to be too strongly deactivating for the catalyst.

a. Reaction conditions
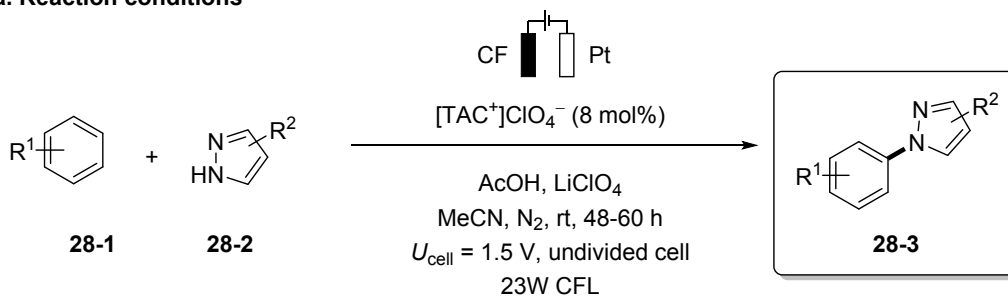
28-1 **28-2** **28-3**

b. Proposed reaction mechanism

c. Representative examples

28-8, 65%

28-9, 46%
(*p*:*o* = 10:1)

28-10, 83%

28-11, 58%
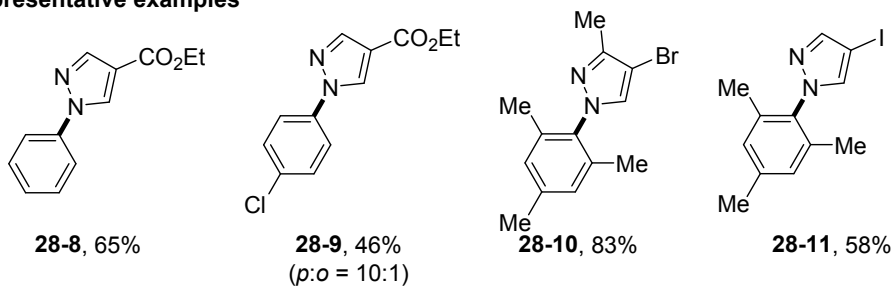
Figure 28. Electrophotocatalytic *N*-arylation of azole with unactivated benzene and aryl halides; a. reaction conditions b. proposed reaction mechanism c. representative examples. [62]

In a recent report, Shen et al demonstrated that TAC⁺ could also be utilized to perform vicinal C-H diamination reactions to form 1,2-diamine derivatives.[58] This is significant because historically, existing strategies for the conversion of C-H to C-N bonds can only accomplish the reaction at a single C-H site. The ideal reaction conditions are shown in Figure 29a. The proposed mechanism is highlighted in Figure

29b and is similar to that shown in Figure 28b; photoexcitation of the TAC radical dication triggers the reaction cascade. Notably, the mechanism for the second amination is not as certain as the first, and it is speculated that the Ritter product **29-7** produces alpha-methylstyrene **29-8** via a reversible acid-catalyzed elimination reaction. Single electron oxidation of **29-8** to **29-9** would then allow the reaction to proceed to product formation. As demonstrated in Figure 29a, depending on the electrolyte used, the product can be either dihydroimidazole **29-2** or aziridine **29-3**.

a. Reaction conditions
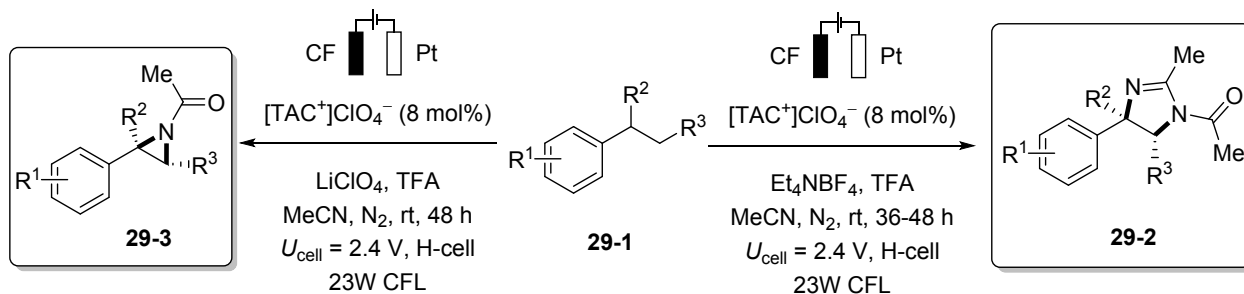
b. Proposed reaction mechanism

First amination
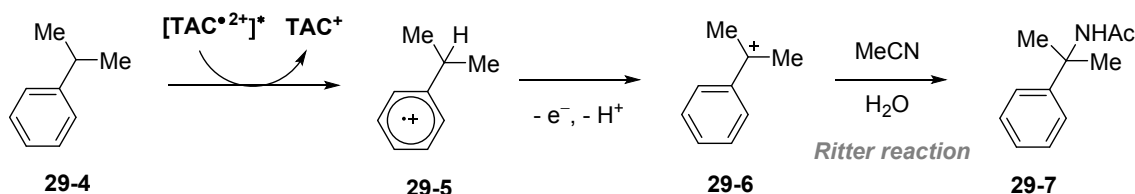
Second amination
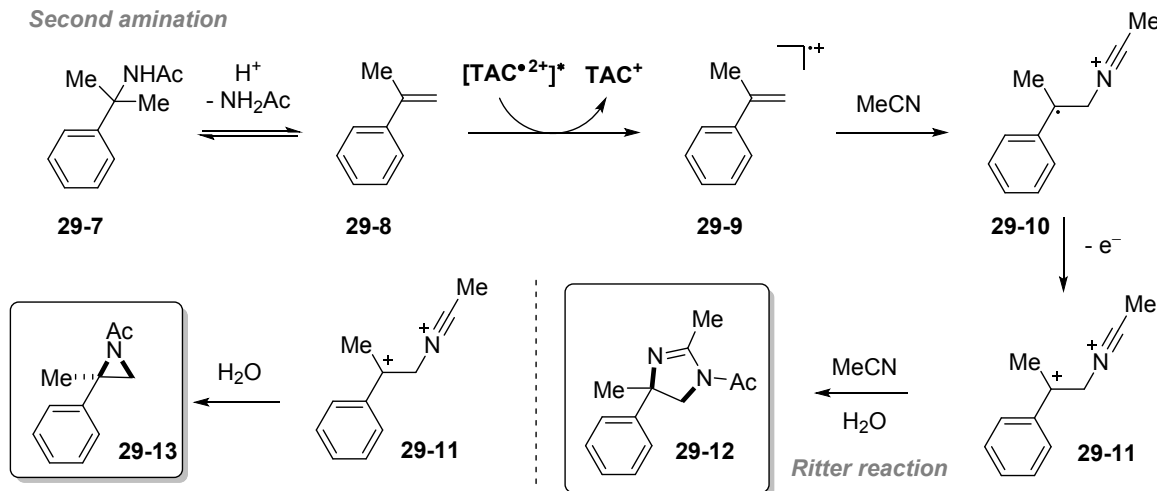
Figure 29. Double C–H amination of ethylbenzene under electrophotocatalytic conditions; a. reaction conditions b. proposed reaction mechanism. [58]

4. Other C–heteroatom bond formation

Over the past few years, there has been a significant interest in electrochemical radical coupling reactions to enable the generation of C–O, C–S, C–N, C–P, and C–halogen bonds.[7, 19] However, most examples are reported to mechanistically proceed through the formation of non-carbon radicals or are non-catalytic. In this section, we summarize the most recent advances in C–heteroatom bond formation that involve electrogenerated carbon-centered radical species.

Stahl and co-workers developed an electrochemical N-hydroxyphthalimide-mediated (NHPI) C–H iodination of methylarenes under mild conditions (Figure 30).[63] NHPI is well known to undergo proton-coupled oxidation at the anode to generate phthalimido-N-oxyl (PINO), which then mediates hydrogen-atom transfer (HAT) from activated benzylic C−H bonds.[55] The formed C–radicals can then be trapped by molecular iodine to generate benzyl iodide coupling products in 40–83% yields. Additionally, the benzyl iodide product can further be trapped by a nucleophile like pyridine to furnish benzylpyridinium derivatives, which serve as precursor to some valuable pyrido-fused N-heterocycles.[64]
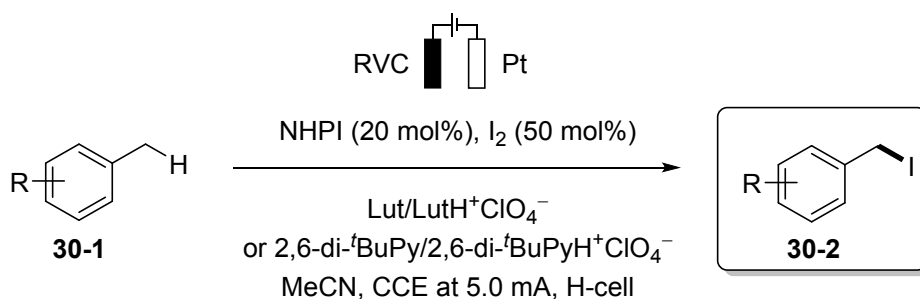
Figure 30. Electro-oxidative iodination of methylarenes mediated by N-hydroxyphthalimide (NHPI).[63] Lut = 2,6-Lutidine. 2,6-di-tBuPy = 2,6-di-*tert*-butylpyridine. RVC = reticulated vitreous carbon.

In 2020, Kim et al developed an electrophotochemical method for reductive functionalization of aryl halides with the use of DCA (9,10-dicyanoanthracene) as an electrophotocatalyst (Figure 31).[35] The **DCA** catalyst is first electro-primed at the cathode prior to photoexcitation to generate the excited species **[DCA•⁻]***(E^{red*} ≈ -3.50 V vs Fc/Fc⁺). This highly reducing radical anion can then donate an electron to the π-system of the aryl halide **31-1** to produce the radical anion **31-3** and regenerate the **DCA** catalyst. Subsequent dehalogenation and trapping of intermediate **31-3** with $B_2(pin)_2$, $Me_3Sn–SnMe_3$, or (hetero)arene leads to the formation of synthetically valuable boronate, organotin, and heterocycle products (Figure 31b). Pyridine was used as an additive to promote the formation of the C–B coupling product, by coordinating to B_2pin_2 to form a B-centered persistent radical adduct. Aryl bromides exhibit high reactivity compared to the chloride counterparts, presumably due to the back electron transfer from the corresponding radical anion to **DCA** (Figure 31c).

a. Reaction conditions
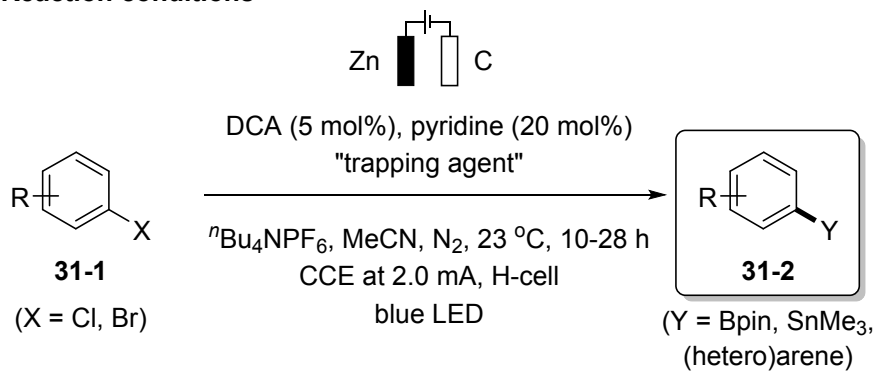
trapping agent = B_2pin_2 $Me_3Sn-SnMe_3$ (Het)ArH

b. Proposed reaction mechanism

c. Representative examples

31-4, 88% (X = Cl)   **31-5**, 17% (X = Cl)   **31-6**, 60% (X = Cl)   **31-7**, 61% (X = Cl)
   90% (X = Br)   46% (X = Br)
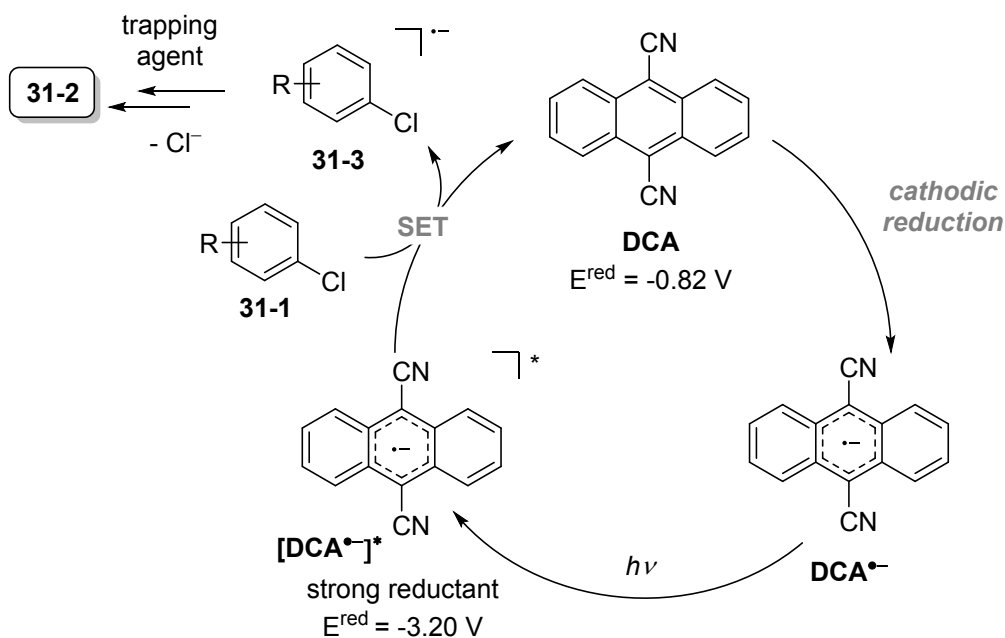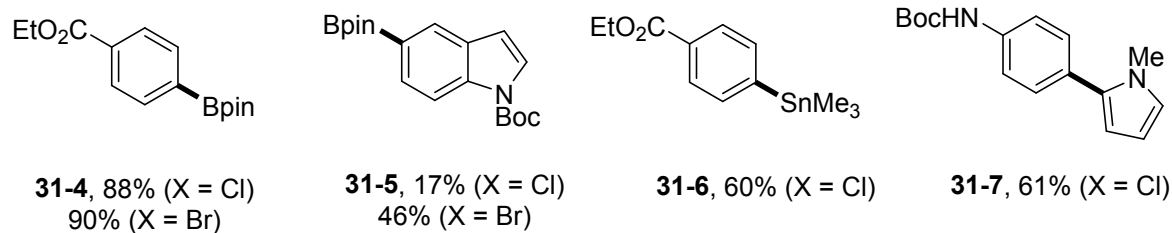
Figure 31. Electrophotocatalysis for reductive functionalization of aryl halides a. reaction conditions b. proposed reaction mechanism c. representative examples.[35]

5. Fixation of CO_2 by Electrocatalysis

Carbon radical chemistry also drives a variety of electrochemical CO_2 fixation reactions, in which CO_2 is reduced and incorporated into a larger organic product. CO_2 fixation has drawn interest due to the pressing environmental need for greenhouse gas mitigation as well as the abundance and low cost of CO_2 as a C_1 source for the generation of value-added products.

Among the simplest C-C bond-forming CO_2 fixation methods is the reduction of CO_2 to oxalate, $C_2O_4^{2-}$, which transforms a C_1 source into a C_2 building block. Across a variety of previously demonstrated electrocatalytic systems, this reaction has long been thought to proceed through a $CO_2^{\bullet-}$ radical intermediate,[65] but the short nanosecond-scale half-life and large dimerization rate constant of $CO_2^{\bullet-}$ render direct detection of the intermediate difficult. More recently, Kai et al have circumvented this issue and demonstrated the ability to directly detect and monitor this radical intermediate en route to oxalate production by using scanning electrochemical microscopy (SECM) at an ultramicroelectrode (UME).[66] As depicted in Figure 32, the $CO_2^{\bullet-}$ generated at a Hg/Pt UME tip with applied negative potential can be collected and reoxidized at an Au UME substrate at a more positive potential, provided that the distance d between the tip and substrate is sufficiently small for $CO_2^{\bullet-}$ to rapidly diffuse to the substrate before undergoing any other reactions. This real-time detection and quantification of the radical intermediate opens the way for further investigation of radical mechanisms in this ongoing research vein. Although Paris and Bocarsly have recently shown reductive electrochemical conversion of CO_2 to oxalate at potentials positive of the thermodynamic potential for CO_2 reduction to $CO_2^{\bullet-}$,[67] radical chemistry continues to play a significant role in many of the reactions reported for this electrochemical transformation.
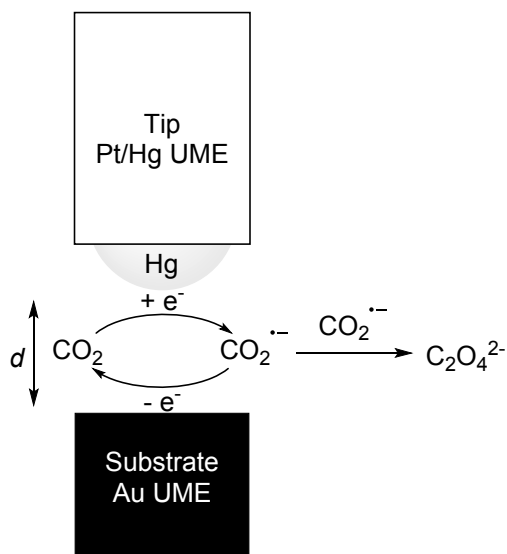
Figure 32. Using the method of Kai et al, $CO_2^{\bullet-}$ generated at a Pt/Hg UME can be detected and quantified at an Au UME substrate provided sufficiently small interelectrode distance d.[66]

Fixation of CO_2 into a larger aromatic product as a carboxylate group has also attracted attention as a renewable and cost-effective transformation. Bazzi et al have demonstrated electrochemical carboxylation of both aryl and benzyl halides from CO_2 using anodically generated Sm complexes.[68, 69] Conditions shown in Figure 33a resulted in successful carboxylation of aryl halides under controlled current conditions in an undivided cell with a sacrificial Sm anode.[68] The reaction proved tolerant to a variety of electron-donating and -withdrawing groups on the substrate, with the exception of para-nitro groups and phenolic substrates thought to coordinate to the Sm^{II} species in solution. Control experiments in the absence of aryl halide

resulted in selective production of oxalic acid, leading the authors to suggest the formation of a Sm^{II}-$CO_2^{\cdot-}$ species **33-3** capable of undergoing either homocoupling to produce oxalate or reaction with aryl halide **33-1** to yield the desired carboxylation product **33-2**. Further supporting the notion of a radical mechanism centered on CO_2, the addition of TEMPO to the solution arrested the reaction while aryl halide starting materials were fully recovered. Notably, non-electrochemical addition of SmX_2 salts directly to solutions of aryl halides did not yield carboxylation products. The proposed mechanism is shown in Figure 33b, in which the required Sm^{II} species is generated at the anode, followed by complexation with CO_2 to yield **33-3**. Reaction with **33-1** yields intermediate **33-4**, which then dissociates from the Sm^{II} complex and is protonated to yield the product **33-2**. In a subsequent report, the carboxylation of benzyl halides to yield phenylacetic acids was found to be similarly effective, this time with the relevant Sm^{II} species being generated anodically before reversing the electrode polarity for electrolysis.[69] Addition of TEMPO in this instance prevented the reaction from proceeding, and lack of formation of benzylated TEMPO adducts suggests once more that a Sm^{II}-$CO_2^{\cdot-}$ radical species could be central to the reaction, similar to the case of the aryl halides, rather than a benzylic radical.
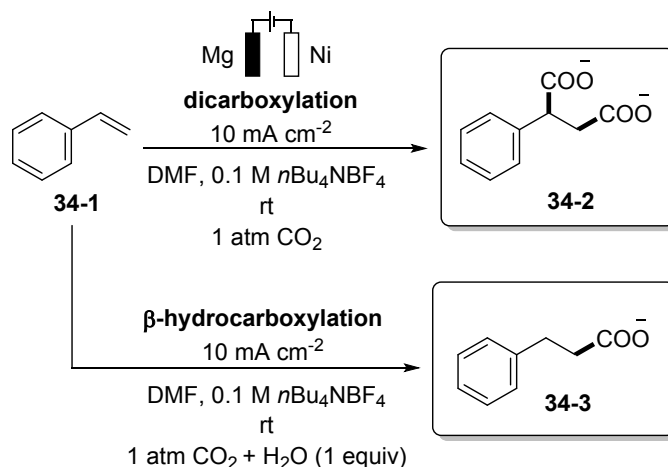
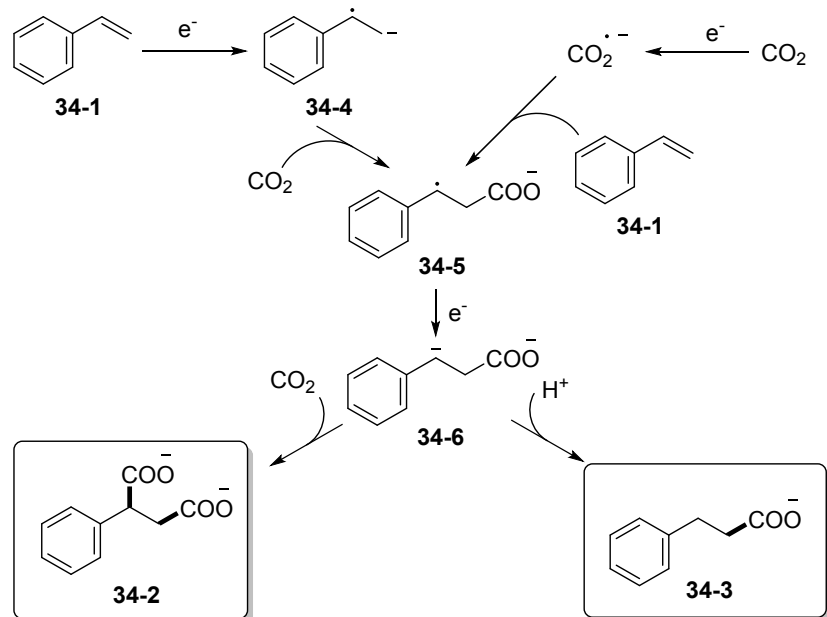**a. Reaction conditions**
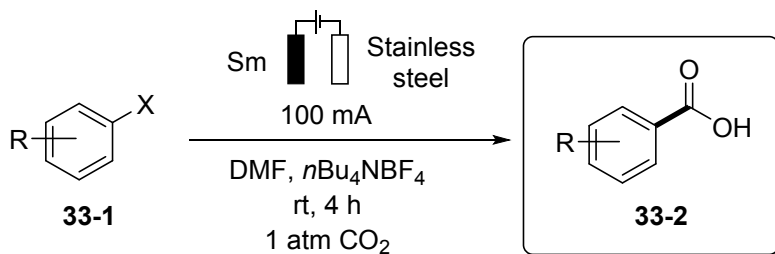
b. Proposed reaction mechanism
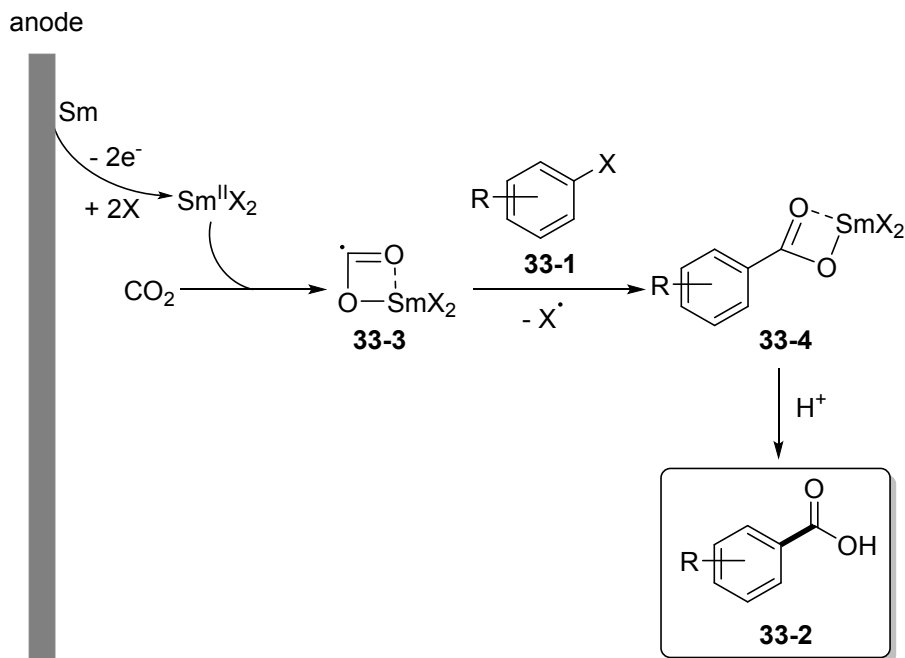
Figure 33. a. Optimized carboxylation conditions of Bazzi et al for carboxylation of aryl halides; b. proposed mechanism.[68]

Similarly, electrochemical (hydro)carboxylation of styrene and related olefins is thought to proceed through carbon radical intermediates. Several authors have investigated the role of radical coupling in these transformations and have been unable to rule out the involvement of $CO_2^{\cdot-}$. For instance, Kim et al found that styrene is successfully carboxylated in the presence of 1 atm CO_2 under controlled current conditions described in Figure 34a.[70] In dry dimethylformamide (DMF), the dicarboxylated product was formed in high yield, while increasing amounts of H_2O as a proton source yielded the β-hydrocarboxylation product in increasing amounts. Tafel analysis of the reaction with varying amounts of H_2O additive from 0 to 0.1 M yielded Tafel slopes of 113 to 120 mV/dec, indicating the involvement of a 1 e^- transfer in the RDS. This is consistent with possible rate-determining formation of $CO_2^{\cdot-}$ or a styrene radical anion. Addition of radical scavengers TEMPO and DMPO appeared to inhibit the production of the dicarboxylation product, while Faradaic efficiencies for the β-hydrocarboxylation product remained largely unaffected relative to the scavenger-free case (68% with TEMPO vs 65% without) or even increased (86% with DMPO). With this information in hand, the authors propose the mechanism outlined in Figure 34b, whereby the reaction may be initiated through a one-electron reduction of CO_2 to $CO_2^{\cdot-}$ or of styrene (**34-1**) to **34-4**. The reaction of either radical with its counterpart ($CO_2^{\cdot-}$ with styrene or **34-4** with CO_2) then results in production of **34-5**. A subsequent one-electron reduction then yields shared intermediate **34-6**, which may then be protonated to yield hydrocarboxylation product **35-3** or react with CO_2 to form dicarboxylation product **34-2**. Although the reaction pathways for both products may proceed through shared intermediates **34-5** and **35-6**, the differential effect of radical scavengers on the Faradaic efficiency for each product suggest that the dicarboxylation reaction follows a pathway that requires additional radical intermediates or otherwise more sensitive radical chemistry. For instance, the dicarboxylation and hydrocarboxylation reactions may proceed through different initial steps (lefthand vs righthand pathway in Figure 34b), or the dicarboxylation reaction may involve direct coupling of $CO_2^{\cdot-}$ to **34-5**. Thus, although the (hydro)carboxylation of styrene under these conditions may theoretically proceed without ever involving direct C-C radical coupling, the possible involvement of $CO_2^{\cdot-}$ cannot be ruled out and may be especially likely in the case of dicarboxylation.

a. Reaction conditions

b. Proposed reaction mechanism

Figure 34. a. Optimized reaction conditions of Kim et al. b. Proposed mechanisms for carboxylation and dicarboxylation. As shown by the dashed arrow, we posit that the differential effect of radical scavengers on the formation of the two products **34-2** and **34-3** may support a pathway for dicarboxylation that does not proceed through the same intermediate **34-6** as the hydrocarboxylation pathway.[70]

Alkayal et al subsequently examined the hydrocarboxylation of styrene-related compounds with a wide substrate scope, including even di- and tri-substituted alkenes (Figure 35).[71] The standard conditions produced highly regioselective β-hydrocarboxylation regardless of the electron-withdrawing or -donating ability of R, with minimal α-hydrocarboxylation side products (β:α ratios of select examples presented in Figure 35c). The conditions proved to be tolerant of a wide variety of R groups, with the exception of R = OH, R = NH$_2$, and R = Br. Similar to the findings of Kim et al, CO$_2$·⁻ cannot be ruled out due to the similar reduction potentials of CO$_2$ and the olefin substrates. The authors thus propose two plausible mechanisms shown as Route A and Route B in Figure 35b, similar to the results of Kim et al, where neither pathway can be definitively disproven.

a. Reaction conditions

35-1 → **35-2**

10 V

DMF, 0.1 M Et_4NI (0.5 equiv)
TEOA (1.0 equiv)
rt, 3.5 h
1 atm CO_2

b. Proposed reaction mechanism

Route A

35-2 ← **35-3** ← **35-1** ← $CO_2^{\cdot-}$ ← CO_2

Route B

35-2 ← **35-5** ← **35-4**

cathode

c. Representative examples

35-6
70%
($\beta:\alpha$ = 8:1)

35-7
96%
($\beta:\alpha$ = 55:1)

35-8
66%
($\beta:\alpha$ = 8:1)

35-9
85%
($\beta:\alpha$ = 11:1)

35-10
82%
($\beta:\alpha$ > 99:1)

35-11
70%

35-12
60%
($\beta:\alpha$ = 2:1)

35-13
60%
($\beta:\alpha$ = 2:1)
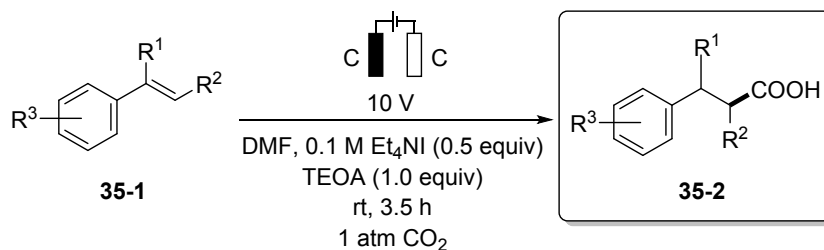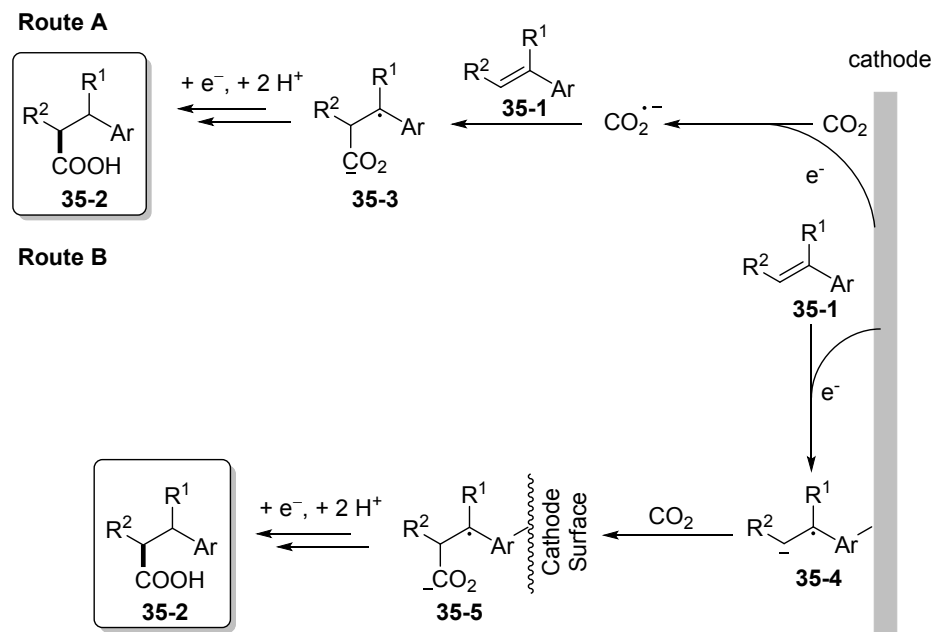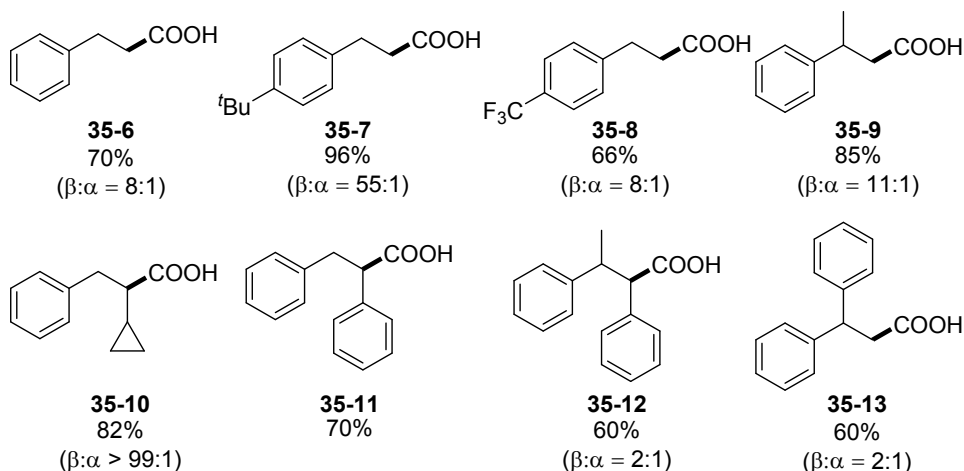
Figure 35. a. Optimized reaction conditions of Alkayal et al.[71] b. Mechanistic proposals based upon the possibility of initial reduction of CO_2 (Route A) and initial reduction of **35-1** (Route B). c. Representative examples of reaction results obtained by varying the identity of one or more of R^1, R^2, and R^3 in the substrate, including notable di- and trisubstituted substrates.

Finally, electrochemical CO_2 fixation has also been investigated in the context of C-N bond-forming reactions. In particular, many electrochemical reactions for the synthesis of urea from CO_2 and N_2 or NO_3^{2-} have been investigated, primarily operating through the use of heterogeneous catalysts.[72] Many existing mechanistic proposals posit that product formation occurs from surface-adsorbed *NH_2 or *CO species, or alternatively *NH_2 and *COOH. In the work of Wang et al, urea formation from heterogeneous PdCu alloy nanoparticles on an oxygen vacancy-rich TiO_2 surface was proposed to occur through a "tower-like" surface-adsorbed *NCON* intermediate, consistent with DFT studies and intermediates observed via isotopically confirmed synchrotron radiation FTIR spectroelectrochemistry.[73] However, such mechanisms are still a topic of debate. Notably, the work of Comer et al has shown that adventitious C radicals on the surface of TiO_2 play an important role in the e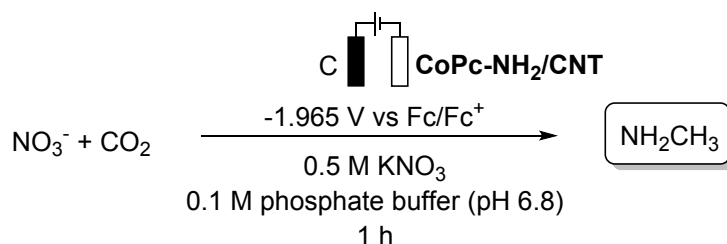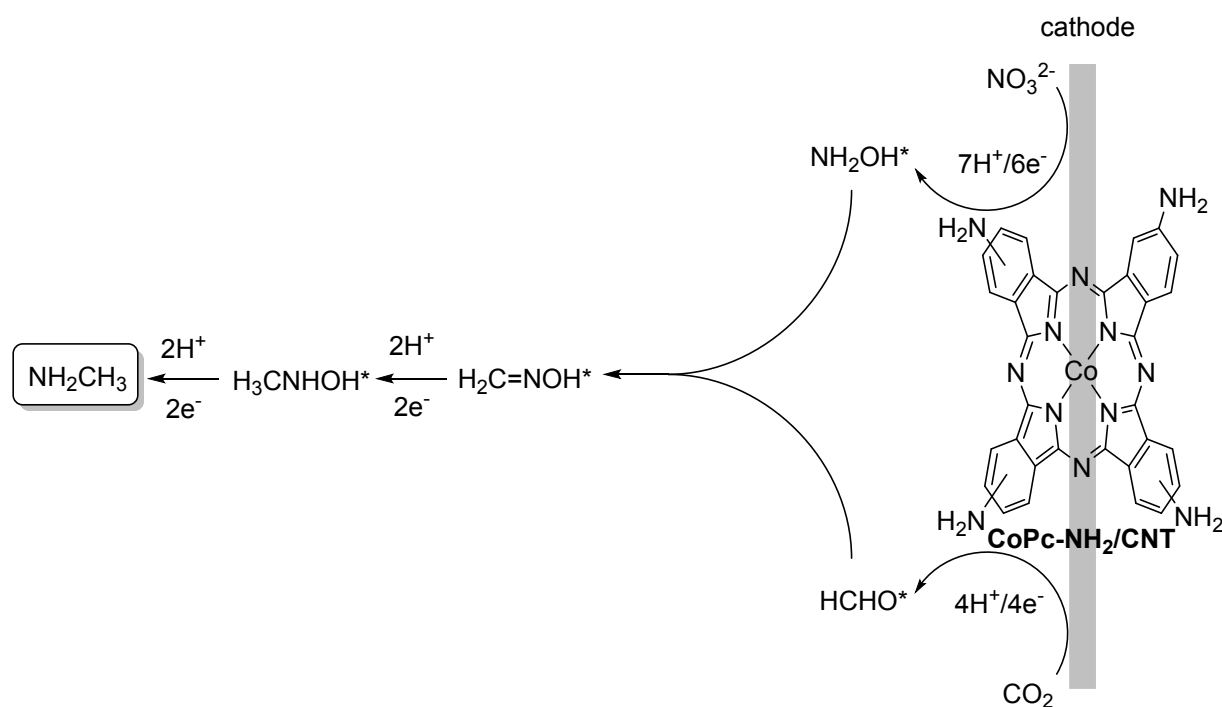lectrochemical fixation of N_2 to ammonia, rather than often-cited oxygen vacancies.[74] Therein, metastable adsorbed *C radical species were found through a combination of experimental and DFT results to be plausible agents for N_2 adsorption and reduction on heterogeneous catalysts in scenarios where adventitious carbon is possible.

Additionally, beyond urea formation, Wu et al have reported the direct electrocatalytic fixation of CO_2 into methylamine.[75] The heterogeneous carbon nanotube (CNT) surface-attached Co phthalocyanine (**CoPc-NH₂/CNT**) molecular catalyst shown in Figure 36 is the first known example for the electrochemical conversion of nitrate and CO_2 into methylamine in aqueous media under ambient conditions. The catalyst had been previously shown to successfully catalyze electrochemical CO_2 reduction to methanol, with CO as an intermediate reduction product,[76] consistent with other studies of electrochemical reduction of CO_2 using CoPc catalysts.[77] Furthermore, **CoPc-NH₂/CNT** also catalyzes the reduction of NO_3^- to NH_3 with NO_2^- and NH_2OH intermediates detected. Thus, the production of methylamine was hypothesized to occur through simultaneous reduction of CO_2 and NO_3^- followed by interaction of intermediates from each independent pathway. To probe the mechanism and identify plausible intermediates, the C and N sources for the reaction were systematically replaced with known intermediates of CO_2 and NO_3^- reduction by the complex. Several such intermediates or reduction products produced methylamine when co-reduced with the other starting material using the catalyst, but NH_3 and NH_4^+ were found to be ineffective as N sources, while methanol was ruled out as a C source. Hydroxylamine and formaldehyde were therefore determined to be the most likely N and C sources for the reaction, respectively, on the basis of nucleophilicity, successful reductions using these two reagents as the starting material, and the detection of formaldoxime and N-methylhydroxylamine in the reaction mixture.[75] The resulting mechanistic proposal is presented in Figure 36b. Additionally, the related **CoPc/CNT** without -NH_2 decoration[78] has been shown to convert a variety of N-nucleophiles + CO_2 to C-N coupling products under similar conditions, showing the ability of this catalytic platform to address a wider scope of substrates and organic products.

a. Reaction conditions

$$NO_3^- + CO_2 \xrightarrow[\substack{0.5 \text{ M KNO}_3 \\ 0.1 \text{ M phosphate buffer (pH 6.8)} \\ 1 \text{ h}}]{\substack{\text{C} \quad \text{CoPc-NH}_2\text{/CNT} \\ -1.965 \text{ V vs Fc/Fc}^+}} NH_2CH_3$$

b. Proposed reaction mechanism

Figure 36. Conversion of CO_2 and NO_3^- to methylamine and proposed mechanism as described by Wu et al,[75] including a. reaction conditions at -1.965 V vs Fc/Fc$^+$ (originally reported as -0.94 V vs RHE) and b. proposed reaction mechanism for the cascade reaction. *denotes species on or near the electrode surface.

5. Summary and outlook

The resurgence of interest in electrochemical methods over the past few years has been punctuated by novel chemistries that repurposed some of the traditional redox reagents towards new chemical reactions. Significant advances have been made towards the electrochemical regeneration of highly reactive redox reagents and new chemistries continue to emerge at the interface of material science, inorganic and organic chemistry. We remain forward looking to advances in the knowledge and mechanistic understanding of radical-enabled use of organic redox mediators to perform new types of chemical reactions that span the research fields of solar fuels and chemical synthesis for pharmaceutical applications.

1.   O. R. Luca, J. L. Gustafson, S. M. Maddox, A. Q. Fenwick and D. C. Smith, *Organic Chemistry Frontiers*, 2015, **2**, 823-848.
2.   R. Francke and R. D. Little, *ChemElectroChem*, 2019, **6**, 4373-4382.
3.   N. Elgrishi, K. J. Rountree, B. D. McCarthy, E. S. Rountree, T. T. Eisenhart and J. L. Dempsey, *Journal of chemical education*, 2018, **95**, 197-206.
4.   E. S. Rountree, B. D. McCarthy, T. T. Eisenhart and J. L. Dempsey, *Journal*, 2014, **53**, 9983-10002.
5.   A. Dey, T. B. Gunnoe and V. R. Stamenkovic, *ACS Catalysis*, 2020, **10**, 13156-13158.
6.   C. C. L. McCrory, S. Jung, J. C. Peters and T. F. Jaramillo, *Journal of the American Chemical Society*, 2013, **135**, 16977-16987.
7.   Y. Yuan, J. Yang and A. Lei, *Chemical Society Reviews*, 2021, **50**, 10058-10086.
8.   L. F. T. Novaes, J. Liu, Y. Shen, L. Lu, J. M. Meinhardt and S. Lin, *Chemical Society Reviews*, 2021, **50**, 7941-8002.
9.   H. Kolbe, *Ann. Chem. Pharm*, 1848, **64**, 339-341.
10.   X. Kong, Y. Liu, L. Lin, Q. Chen and B. Xu, *Green Chemistry*, 2019, **21**, 3796-3801.
11.   Q.-Q. Wang, K. Xu, Y.-Y. Jiang, Y.-G. Liu, B.-G. Sun and C.-C. Zeng, *Organic Letters*, 2017, **19**, 5517-5520.
12.   D.-Z. Lin and J.-M. Huang, *Organic Letters*, 2019, **21**, 5862-5866.
13.   F. Rudolphi, B. Song and L. J. Gooßen, *Advanced Synthesis & Catalysis*, 2011, **353**, 337-342.
14.   X.-L. Lai, X.-M. Shu, J. Song and H.-C. Xu, *Angewandte Chemie International Edition*, 2020, **59**, 10626-10632.
15.   Z.-J. Wu and H.-C. Xu, *Angewandte Chemie International Edition*, 2017, **56**, 4734-4738.
16.   Z.-J. Wu, S.-R. Li, H. Long and H.-C. Xu, *Chemical Communications*, 2018, **54**, 4601-4604.
17.   B. B. Snider, *Chemical Reviews*, 1996, **96**, 339-364.
18.   Z.-J. Wu, S.-R. Li and H.-C. Xu, *Angewandte Chemie International Edition*, 2018, **57**, 14070-14074.
19.   H. Wang, X. Gao, Z. Lv, T. Abdelilah and A. Lei, *Chemical Reviews*, 2019, **119**, 6769-6787.
20.   G.-X. Li, X. Hu, G. He and G. Chen, *ACS Catalysis*, 2018, **8**, 11847-11853.
21.   X.-A. Liang, L. Niu, S. Wang, J. Liu and A. Lei, *Organic Letters*, 2019, **21**, 2441-2444.
22.   A. Hu, J.-J. Guo, H. Pan and Z. Zuo, *Science*, 2018, **361**, 668-672.
23.   S. Caron, R. W. Dugger, S. G. Ruggeri, J. A. Ragan and D. H. B. Ripin, *Chemical Reviews*, 2006, **106**, 2943-2989.
24.   P. Xu, P.-Y. Chen and H.-C. Xu, *Angewandte Chemie International Edition*, 2020, **59**, 14275-14280.
25.   H. Huang, Z. M. Strater and T. H. Lambert, *Journal of the American Chemical Society*, 2020, **142**, 1698-1703.
26.   L. Song, N. Fu, B. G. Ernst, W. H. Lee, M. O. Frederick, R. A. DiStasio and S. Lin, *Nature Chemistry*, 2020, **12**, 747-754.
27.   K.-Y. Ye, G. Pombar, N. Fu, G. S. Sauer, I. Keresztes and S. Lin, *Journal of the American Chemical Society*, 2018, **140**, 2438-2441.
28.   K.-Y. Ye, Z. Song, G. S. Sauer, J. H. Harenberg, N. Fu and S. Lin, *Chemistry – A European Journal*, 2018, **24**, 12274-12279.
29.   G. A. Molander, *The Journal of Organic Chemistry*, 2015, **80**, 7837-7848.

30.   K. Duan, X. Yan, Y. Liu and Z. Li, *Advanced Synthesis & Catalysis*, 2018, **360**, 2781-2795.
31.   H. Yan, Z.-W. Hou and H.-C. Xu, *Angewandte Chemie International Edition*, 2019, **58**, 4592-4595.
32.   G.-X. Li, C. A. Morales-Rivera, Y. Wang, F. Gao, G. He, P. Liu and G. Chen, *Chemical Science*, 2016, **7**, 6407-6412.
33.   S. Castro, J. J. Fernández, F. J. Fañanás, R. Vicente and F. Rodríguez, *Chemistry – A European Journal*, 2016, **22**, 9068-9071.
34.   Y. Yuan, Y. Zheng, B. Xu, J. Liao, F. Bu, S. Wang, J.-G. Hu and A. Lei, *ACS Catalysis*, 2020, **10**, 6676-6681.
35.   H. Kim, H. Kim, T. H. Lambert and S. Lin, *Journal of the American Chemical Society*, 2020, **142**, 2087-2092.
36.   D. S. P. Cardoso, B. Šljukić, D. M. F. Santos and C. A. C. Sequeira, *Organic Process Research & Development*, 2017, **21**, 1213-1226.
37.   Y. Ma, J. Hong, X. Yao, C. Liu, L. Zhang, Y. Fu, M. Sun, R. Cheng, Z. Li and J. Ye, *Organic Letters*, 2021, **23**, 9387-9392.
38.   J. Luo, B. Hu, W. Wu, M. Hu and T. L. Liu, *Angewandte Chemie International Edition*, 2021, **60**, 6107-6116.
39.   R. J. Perkins, D. J. Pedro and E. C. Hansen, *Organic Letters*, 2017, **19**, 3755-3758.
40.   R. C. Samanta, J. Struwe and L. Ackermann, *Angewandte Chemie International Edition*, 2020, **59**, 14154-14159.
41.   V. V. Grushin and H. Alper, *Chemical Reviews*, 1994, **94**, 1047-1062.
42.   A. F. Littke and G. C. Fu, *Angewandte Chemie International Edition*, 2002, **41**, 4176-4211.
43.   S. Kim, M. J. Goldfogel, M. M. Gilbert and D. J. Weix, *Journal of the American Chemical Society*, 2020, **142**, 9902-9907.
44.   M. J. Goldfogel, L. Huang and D. J. Weix, in *Nickel Catalysis in Organic Synthesis*, 2020, DOI: https://doi.org/10.1002/9783527813827.ch9, pp. 183-222.
45.   H. G. Roth, N. A. Romero and D. A. Nicewicz, *Synlett*, 2016, **27**, 714-723.
46.   A. Matsunaga and A. Yasuhara, *Chemosphere*, 2005, **58**, 897-904.
47.   N. G. W. Cowper, C. P. Chernowsky, O. P. Williams and Z. K. Wickens, *Journal of the American Chemical Society*, 2020, **142**, 2093-2099.
48.   H. Li, C. P. Breen, H. Seo, T. F. Jamison, Y.-Q. Fang and M. M. Bio, *Organic Letters*, 2018, **20**, 1338-1341.
49.   T. Koyanagi, A. Herath, A. Chong, M. Ratnikov, A. Valiere, J. Chang, V. Molteni and J. Loren, *Organic Letters*, 2019, **21**, 816-820.
50.   F. Lian, K. Xu, W. Meng, H. Zhang, Z. Tan and C. Zeng, *Chemical Communications*, 2019, **55**, 14685-14688.
51.   S. Zhang, L. Li, X. Li, J. Zhang, K. Xu, G. Li and M. Findlater, *Organic Letters*, 2020, **22**, 3570-3575.
52.   B. Zhang, X. Qu, J. Qu, X. Chen, H. Xie, P. Xing, D. Wang and H. Yin, *Green Chemistry*, 2020, **22**, 8633-8641.
53.   E. Steckhan, T. Arns, W. G. Heineman, D. Hoormann, J. Jörissen, L. Kröner, B. Lewall and H. Pütter, *Chemosphere*, 2001, **43**, 63-73.
54.   F. Schendzielorz, M. Finger, J. Abbenseth, C. Würtele, V. Krewald and S. Schneider, *Angewandte Chemie International Edition*, 2019, **58**, 830-834.
55.   J. E. Nutting, M. Rafiee and S. S. Stahl, *Chemical Reviews*, 2018, **118**, 4834-4885.
56.   A. G. Bakhoda, S. Wiese, C. Greene, B. C. Figula, J. A. Bertke and T. H. Warren, *Organometallics*, 2020, **39**, 1710-1718.
57.   L. Niu, C. Jiang, Y. Liang, D. Liu, F. Bu, R. Shi, H. Chen, A. D. Chowdhury and A. Lei, *Journal of the American Chemical Society*, 2020, **142**, 17693-17702.
58.   T. Shen and T. H. Lambert, *Science*, 2021, **371**, 620-626.

59.   D.-Z. Lin and J.-M. Huang, *Organic Letters*, 2018, **20**, 2112-2115.
60.   H. Huang and T. H. Lambert, *Angewandte Chemie International Edition*, 2020, **59**, 658-662.
61.   H. Huang and T. H. Lambert, *Angewandte Chemie International Edition*, 2021, **60**, 11163-11167.
62.   H. Huang, Z. M. Strater, M. Rauch, J. Shee, T. J. Sisto, C. Nuckolls and T. H. Lambert, *Angewandte Chemie International Edition*, 2019, **58**, 13318-13322.
63.   M. Rafiee, F. Wang, D. P. Hruszkewycz and S. S. Stahl, *Journal of the American Chemical Society*, 2018, **140**, 22-25.
64.   Y. Liu, H. Hu, J. Zhou, W. Wang, Y. He and C. Wang, *Organic & Biomolecular Chemistry*, 2017, **15**, 5016-5024.
65.   C. Costentin, M. Robert and J.-M. Savéant, *Chemical Society Reviews*, 2013, **42**, 2423-2436.
66.   T. Kai, M. Zhou, Z. Duan, G. A. Henkelman and A. J. Bard, *Journal of the American Chemical Society*, 2017, **139**, 18552-18557.
67.   A. R. Paris and A. B. Bocarsly, *ACS Catalysis*, 2019, **9**, 2324-2333.
68.   S. Bazzi, G. Le Duc, E. Schulz, C. Gosmini and M. Mellah, *Organic & Biomolecular Chemistry*, 2019, **17**, 8546-8550.
69.   S. Bazzi, E. Schulz and M. Mellah, *Organic Letters*, 2019, **21**, 10033-10037.
70.   Y. Kim, G. D. Park, M. Balamurugan, J. Seo, B. K. Min and K. T. Nam, *Advanced Science*, 2020, **7**, 1900137.
71.   A. Alkayal, V. Tabas, S. Montanaro, I. A. Wright, A. V. Malkov and B. R. Buckley, *Journal of the American Chemical Society*, 2020, **142**, 1780-1785.
72.   Z. Tao, C. L. Rooney, Y. Liang and H. Wang, *Journal of the American Chemical Society*, 2021, **143**, 19630-19642.
73.   J. Wang, P. Qian, K. Hu, Z. Zha and Z. Wang, *ChemElectroChem*, 2019, **6**, 4292-4296.
74.   B. M. Comer, Y.-H. Liu, M. B. Dixit, K. B. Hatzell, Y. Ye, E. J. Crumlin, M. C. Hatzell and A. J. Medford, *Journal of the American Chemical Society*, 2018, **140**, 15157-15160.
75.   Y. Wu, Z. Jiang, Z. Lin, Y. Liang and H. Wang, *Nature Sustainability*, 2021, **4**, 725-730.
76.   Y. Wu, Z. Jiang, X. Lu, Y. Liang and H. Wang, *Nature*, 2019, **575**, 639-642.
77.   E. Boutin, M. Wang, J. C. Lin, M. Mesnage, D. Mendoza, B. Lassalle-Kaiser, C. Hahn, T. F. Jaramillo and M. Robert, *Angewandte Chemie International Edition*, 2019, **58**, 16172-16176.
78.   C. L. Rooney, Y. Wu, Z. Tao and H. Wang, *Journal of the American Chemical Society*, 2021, **143**, 19983-19991.